Longer heatwaves disrupt bacterial communities by decoupling resistance from recovery

Ana-Hermina Ghenu[1], Anjaney J. Pandey[1,2,4], Zachary M. Bailey[1], David R. Johnson[1,3] and Madhav P. Thakur[1]

May 1, 2025

[1]Institute of Ecology and Evolution, University of Bern, Bern, Switzerland
[2]Department of Bioengineering, Indian Institute of Science, Bangalore, India
[3]Department of Environmental Microbiology, Swiss Federal Institute of Aquatic Science and Technology (Eawag), Dübendorf, Switzerland
[4]Undergraduate Programme, Indian Institute of Science, Bangalore, India

Authors' contributions.

AHG: Conceptualization, Methodology, Validation, Formal analysis, Investigation, Resources, Data Curation, Writing - Original Draft, Writing - Review & Editing, Visualization, Supervision, Project administration.

AJP: Validation, Formal analysis, Investigation, Writing - Review & Editing.

ZMB: Formal analysis, Investigation, Resources, Writing - Original Draft, Visualization.

DRJ: Methodology, Writing - Review & Editing, Supervision.

MPT: Conceptualization, Methodology, Writing - Original Draft, Writing - Review & Editing, Supervision, Project administration, Funding acquisition.

Funding. SNF project grant 310030_212550 awarded to MPT. ThinkSwiss Research Scholarship awarded to AJP.

Acknowledgements. Members of the Terrestrial Ecology Division University of Bern, including Silvia Brochet (16S sequencing and species identification), Gerard Martínez-De León (stats discussion), Nicholas Tartini (stats discussion), and Anine Wiser (data collection). Chujin Ruan at Eawag (species interactions pilot experiment). Vladimir Senchillo at University of Lausanne (fluorescent strain construction).

Data accessibility. Most data and complete analyses can be found at https://github.com/EvoNerd/Xtreme_heat. The flow cytometry raw data and FCS Express analysis files can be found at https://figshare.com/projects/Longer_heat_pulses_disrupt_bacterial_communities_by_decoupling_resistance_from_recovery/246812

Subject area. Ecology, Microbiology, Environmental Science.

Keywords. climate change, soil microbes, community ecology, thermal performance traits, heat pulse duration, flow cytometry, ecological decoupling, multispecies interactions, community collapse, congeneric species differences.

Corresponding author. AHG: ana.hermina.ghenu@gmail.com

Longer heatwaves disrupt bacterial communities by decoupling resistance from recovery

Abstract

Periodic heatwaves are increasing in duration, yet their ecological impacts on communities remain poorly understood. We experimentally tested how synthetic communities of soil *Pseudomonas* species respond to heatwaves of increasing duration. We used a resistance-recovery framework and growth rate-heat tolerance trade-offs to predict whether prolonged stress erodes community stability. Communities composed of species with different growth rates were exposed to single heat pulses lasting 6, 12, 24, or 48 hours. Although we expected the fastest-growing and most heat-tolerant species, *P. putida*, to dominate, a species with moderate growth and heat tolerance, *P. protegens*, consistently prevailed. This outcome was likely driven by diffusible toxins and unexpectedly high heat tolerance linked to density-dependent growth. On average, each additional hour of heat exposure increased community extinction risk by 21.5%, with faster-growing communities exhibiting lower risks. The longest heat pulse caused sharp declines in diversity and productivity, leading to greater decoupling between resistance and recovery as well as reduced overall stability. These findings demonstrate that growth rate and species interactions — not heat resistance alone — determine community fate during and after heat stress. Our results highlight the need to incorporate nonlinear dynamics and trait-based interactions when predicting microbial responses to climate extremes.

1 Introduction

Climate change is driving more frequent, intense, and prolonged heatwaves [1]. These extreme events threaten biodiversity by increasing species extinctions, destabilizing communities, and disrupting ecosystem functioning [2, 3]. Yet, little is known about the ecological mechanisms that can destabilize communities during prolonged heatwaves. Understanding how heatwave duration influences community dynamics is crucial for predicting these impacts. Moreover, identifying the mechanisms that determine community stability under such conditions can help predict which species are likely to persist or decline during climate extremes [4]. Here, using soil bacterial communities, we test the roles of growth rates and species interactions in predicting community stability under prolonged heatwaves.

Trait-based ecological approaches provide a promising way to understand the mechanisms of community stability and predict community responses to heatwaves [5]. For instance, a community's stability to various types of perturbation may ultimately depend on the life history strategies of its component species [6]. Life history strategies are defined by the magnitude and co-variation of vital rates such as growth rate, stress resistance, and competitiveness. Slow-growing species are typically excluded by fast-growing species unless there is a trade-off between growth rate and competitiveness [6, 7]. In this case, slow-growing competitive species can exclude others by promoting their own growth, limiting others, and/or resisting environmental stress. For example, plants with a slow life history strategy often exhibit slow growth, high resistance to stress, and competitiveness in acquiring resources [8], which we here refer to as the growth rate-resistance trade-off. Testing the generality of this trade-off across diverse taxa is critical for understanding how life history strategies scale up to influence community stability [9, 10]. Soil bacteria, among the most diverse groups in the biosphere [11], offer a powerful system for evaluating the role of growth rate–resistance trade-offs in shaping community responses to prolonged heatwaves.

Soil bacterial communities control the recycling of up to 50–80% of soil organic matter, which is the Earth's largest actively cycling reservoir of carbon [12]. These communities influence whether soils act as net sinks or sources of greenhouse gases [13]. Therefore understanding the mechanisms of soil bacterial community stability under prolonged heatwaves is crucial for improved climate change predictions. Similar to plants, bacteria are thought to exhibit a growth rate-resistance trade-off, with slow-growing species faring better in extreme environments [14]. However, elevated temperature is a complex stressor [15] and few studies have identified bacterial functional traits that are relevant for community stability during heat [16]. Growth rate and competitiveness tend to be negatively correlated in bacteria, leading to the prevalence of fast-growing species at cooler

temperatures (4–20°C) and slow-growing species at warmer ones (25–30°C). Few studies have investigated how these communities change during and after a prolonged heat pulse ($> 30°C$).

In the laboratory, community stability [17] can be assayed experimentally by decomposing it into two phases: the immediate response to a stress event such as a heat pulse (resistance) and the response after the event subsides (recovery). A community's stability is estimated by measuring the extent of its response during the resistance and recovery phases as compared to an undisturbed control [18, 19]. Stable communities are expected to have a positive correlation, or coupling, between resistance and recovery [20, 21]. Coupling indicates that a community's short-term response can predict its long-term outcome [22–24]. In contrast, decoupling — a significant difference between resistance and recovery responses — indicates less predictability and suggests more complex dynamics, such as ecological trade-offs [3]. For example, increased decoupling of productivity in response to longer heat pulse duration was found in soil animals, where high survival investment during the resistance phase resulted in a trade-off with low fecundity during the recovery phase [25]. At the single-cell level, resistance reflects the extent to which a cell's growth rate declines under stress, whereas recovery reflects the time needed to regain maximum growth after stress release, potentially revealing trade-offs between immediate stress tolerance and post-stress regrowth. Such trade-offs at the cellular level could scale up to influence how entire communities resist, recover, or decouple under prolonged heatwaves. Species richness is another ecological mechanism that impacts decoupling because diverse communities tend to have smaller total productivity responses during both resistance and recovery [26]. Assaying the presence and magnitude of decoupling using a resistance-recovery experimental framework can therefore link the short-term dynamics of bacterial communities to their long-term outcomes.

Here, we conducted two interconnected experiments to test whether species-specific thermal performance traits could predict community responses during and after heat pulses of different duration. The first (Experiment I) measured bacterial thermal performance traits to inform the second experiment (Experiment II), which used a resistance-recovery framework to quantitatively assess the role of biotic interactions under varying heat pulse durations. In Experiment I, we selected 16 strains from six species of soil bacteria from the genus *Pseudomonas* and quantified their growth traits at four temperatures ($25, 30, 35$, and $40°C$). We hypothesized that bacterial species would exhibit a growth rate-resistance trade-off, but we did not observe this. Although we could assign bacterial species to growth rate categories, the fastest growing species *P. putida*, was also the most heat resistant. Given this result, we designed Experiment II with four species across a gradient from fast to slow that retain the same rank order during heat (i.e., no trade-off between growth rate and heat resistance). The communities were inoculated at equal starting ratios in all 15 possible species combinations (i.e., singletons, pairs, triplets, and quadruplet), exposed to a single heat pulse of variable duration (6, 12, 24, or 48 hours (hrs)), then allowed to recover for a fixed two-day duration. We hypothesized that the fastest growing species (*P. putida*) would dominate the communities exposed to the longer heat pulses, as it is also the most heat resistant. For all communities, we hypothesized that intrinsic growth rate and resistance to extreme heat, as measured from monocultures in Experiment I, would predict the composition and productivity of co-culture communities in Experiment II, with this effect becoming stronger with longer heat pulse duration.

2 Materials and methods

2.1 Medium and bacterial strains

LB broth (Lennox formulation) from Carl Roth was used throughout.

16 soil *Pseudomonas* strains from six species were used (Table S1) [27–31]. Samples were colony-PCR amplified, Sanger sequenced for 16S rRNA 27F/907R (corresponding to subregions V1-V5), and identified to the nearest species by BLASTN.

The four focal genotypes of Experiment II have constitutive expression of chromosomally integrated fluorescent proteins and were all built using an established gene delivery vector [32]. Fluorescent proteins were integrated onto the *P. putida* F1 (BSC001; sYFP), *P. protegens* Pf5 (CK101; mTurquoise2), and *P. veronii* (BSC005; mScarlet) backgrounds in previous studies; the

sGFP2 fluorescent genotype of *P. grimontii* (BSC028) [28] was built for this experiment using the Tn7 transposon delivery plasmid [32] (Table S1).

2.2 Experiment I

2.2.1 Thermal performance traits

For each strain, the probability of growth under heat stress was estimated by colony forming units (CFUs). Intrinsic growth rates and the intraspecific density dependence of growth rate were estimated using time-to-detection growth curves [33]. The time-to-detection approach allows estimation of density-independent (i.e., intrinsic) growth rates despite the high threshold of detection of the microplate reader [34].

The time-to-detection protocol was modified for high throughput by snap freezing the inocula into single-use 'shots', either at the stationary or early exponential phase. Bacteria were streaked on LB agar, incubated overnight at $28°C$, and single colonies were inoculated into liquid LB with 225 rpm shaking. For stationary phase inocula, 3.0 mL of media was incubated for 24 hrs, yielding an optical absorbance at 600 nm (OD_{600}) > 3. Then, cultures were resuspended to $OD_{600} = 0.25$ into their own filter-sterilized spent media with 10% glycerol. For early exponential phase inocula, 55 mL of media was incubated to an OD_{600} between 0.01–0.05 ($\sim$ 4–7 hrs) and then resuspended into fresh media with glycerol as above. $100\mu L$ inocula were put in PCR strip-tubes and snap-frozen on dry ice. These single-use inoculum shots were stored at $-79°C$ and used within 2 months. Thawed inocula were diluted into liquid LB to create a six-step, 10-fold dilution series (10^{-1} to 10^{-6}) for CFUs and growth curves.

CFUs were incubated at three temperatures ($28°C$, $35°C$, and $40°C$) using the 6x6 drop plate method [35], with three replicates for each inocula culture phase. Plates were incubated until colonies could be counted by eye (at least overnight) or failed to show discernible growth (at most 7 days).

Growth curves were measured at four temperatures ($25°C$, $30°C$, $35°C$, and $40°C$) using 200μL cultures in 96-well microplates covered with a Breathe-Easy sealing membrane on Agilent BioTek Epoch 2 or Synergy H1 microplate readers with continuous double-orbital shaking at 807 cpm (1 mm) and a vertical heat gradient of $1°C$ to prevent condensation. OD_{600} was measured every 10 min [36] until cultures reached carrying capacity (at least 42 hrs) or failed to show discernible growth (at most 60 hrs). Replicate dilution series were done on three different days for each culture phase, randomizing the incubator and microplate well location.

2.3 Experiment II

2.3.1 Communities' resistance and recovery from extreme heat

As illustrated in Figure 1, bacterial communities were grown in a serial-transfer, batch culture system. Monocultures were inoculated from single colonies into 10mL of liquid media (Day -1) and incubated overnight as described above. The next morning (Day 0), monoculture absolute densities were measured in triplicate by flow cytometry. After adjusting the monoculture densities to an equal value, the four species were combined at equal ratios into all 15 possible communities (n=5) and an estimated 10^3 total cells were inoculated into 125μL of media. The 15 communities were arranged in 5 blocks throughout the 96-well microplate (Figure S1) to randomize any edge effects [37]. The microplate was covered with parafilm and a lid to prevent differential evaporation at $40°C$. Microplates were incubated in Agilent Epoch 2 or Synergy H1 readers with continuous double-orbital shaking at 205 cpm (5 mm) for a day (22–23 hrs) and OD_{600} was acquired regularly. Each day (Days 1–5), 5% of the culture was transferred to fresh medium and the remainder was used to estimate species abundances by flow cytometry.

2.3.2 Estimating species abundances by flow cytometry & identifying community extinctions

Cell counts were recorded using an Invitrogen Attune CytPix flow cytometer with blue/violet/yellow lasers, NxT Fluorescent Protein Filter Kit, NxT Small Particle Side-Scatter Filter, and CytKick

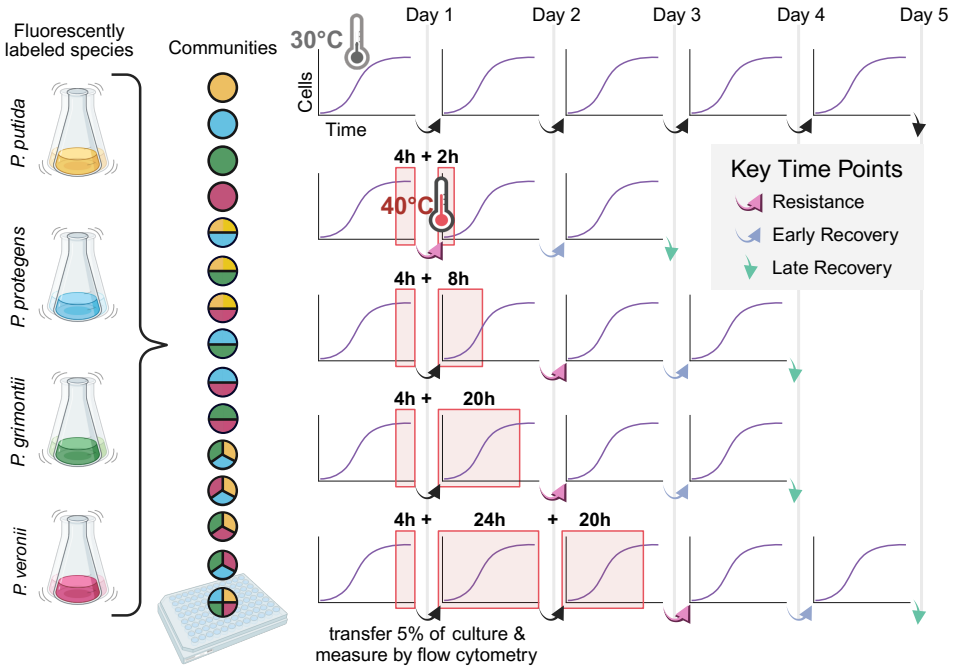

Figure 1: **Design of resistance and recovery experiment with variable heat pulse duration.** Overnight monocultures of four species (Table S1) constitutively expressing sYFP, mTourquoise2, sGFP2, and mScarlet fluorescent proteins (flasks at left) were inoculated at equal ratios in all 15 combinations of communities (coloured circles) into a 96-well microplate. Batch cultures were measured for their species abundances by flow cytometry and transferred daily (arrows). Starting from the end of Day 1, the cultures were exposed to a single $40°C$ heat pulse of variable duration (6, 12, 24, or 48 hrs; highlighted in red) then allowed to recover for two days. Measurements near the end of or just after the heat pulse are referred to as 'resistance' time points (bold pink arrow), while those from the first or second day post-heat are called early or late recovery (purple-blue and turquoise arrows), respectively. Treatments are always compared with the no-heat control on the same day of serial transfer. Figure made with BioRender.

autosampler. Cultures were diluted in 7.52 mM tetrasodium pyrophosphate at pH 7.5 to a concentration of 10^{-3}x for overnight monocultures (Day 0) or 10^{-2}x for all other measurements. Cells were separated from debris using a rectangular gate in side-scatter area and forward-scatter area (Figure S2A). Up to 10^4 events in the bacterial cells gate were sampled from $\leq 146\mu$L of diluted cultures at 25μL/min.

Cell counts and well volumes were extracted from the flow cytometry data using FCS Express (version 7.22.0006) and the Attune Cytometric Software (version 6.1.1), respectively, to estimate event densities. Events from the cells gate were classified into four fluorophore-specific subsets (Figure S2B-E) using four sets of three nested polygonal gates in the fluorescent channel heights (these gates were also used to exclude doublets). As each species expresses a unique fluorophore, this allowed us to estimate species-specific cell counts. Absolute species abundances were estimated by dividing the flow cytometry cell counts by the acquired well volume. Flow cytometry raw data and estimation of cell counts can be found at these anonymous review links: https://figshare.com/s/d81c927071951ba776e7, https://figshare.com/s/4fbdd4550e7a16752044, https://figshare.com/s/183d7cb990b1e2ab76a8, https://figshare.com/s/cb37922b5ebabc628642, and https://figshare.com/s/fd044109578f5c582c81.

The threshold of detection of the flow cytometer is operationally defined as 50 events in the bacterial cell gate, which is more than twice the maximum number of events that we recorded for a true blank.

The serial-transfer OD_{600} growth data was used to estimate the rate of contamination and to verify extinction events. Contamination was inferred to have occurred in well blanks whose

baseline-subtracted OD_{600} surpassed the maximum value observed for a true blank (Figure S3A). Extinction was inferred to have occurred for community replicates where the baseline-subtracted OD_{600} on the last day of recovery never surpassed the maximum value for uncontaminated well blanks (Figure S3B). Extinction events corresponded with flow cytometer cell counts below the threshold of detection.

2.3.3 Assaying diffusible species interactions

P. protegens, *P. putida*, *P. grimontii*, and *P. veronii* (hereafter the focal species) were grown in co-cultures with *P. protegens* in 25 mL flasks for 24 hours at 220 rpm and $30°C$. These cultures were centrifuged at 10 000 g for five minutes, the supernatant was removed, filtered twice using a 0.22 μm PES filter, and plated on agar plates to verify the absence of live bacteria. This supernatant was mixed with fresh media and aliquoted to 96-well microplates so that each focal species could be subjected to 90%, 80%, 70%, 60%, 50%, 40%, 30%, 20%, 10% , 5%, and 0% of each supernatant. The OD_{600} of each population was measured over 12 hrs with a BioTek plate reader. The final versus initial OD_{600} values were compared to determine the effect of diffusible secondary metabolites produced by *P. protegens* on focal species' growth. The inhibitory concentration, defined as the concentration that reduces the population size by 50% (IC_{50}), was estimated for each focal species by nonlinear least squares fitting using the nlsLM function (minpack.lm [38]) initialized in R with a Hill curve function.

2.4 Statistical analyses

All statistical analyses were performed in R (version 4.4.2 [39]). The data and code for the analysis of both experiments (except flow cytometry raw data and estimation of cell counts) is provided at this anonymous GitHub link: `https://anonymous.4open.science/r/Xtreme_heat-358A/`.

For Experiment I, the growth rates were estimated from the interpolated baseline-subtracted optical absorbance data in the mid-exponential phase (time-to-detection threshold $OD_{600} = 0.05$), the estimated inoculum size from CFUs, and calibration curves for each microplate reader [40]. Intraspecific density dependence was estimated as per-capita derivatives from gcplyr (version 1.10.0 [41]). To test for a correlation between the growth rates at ambient temperatures ($25°C$ or $30°C$) with the species' growth traits (intrinsic growth rate or probability of growth by CFU) at extreme heat ($40°C$), we used both a parametric approach with linear mixed models as well as a non-parametric approach with the species rankings.

For Experiment II, species abundances were analyzed at three key time points (Figure 1): 'resistance' (last day of the heat pulse), 'early recovery' (first day post-heat), and 'late recovery' (second day post-heat). Ordination analysis by non-metric multidimensional scaling (NMDS; vegan, version 2.6.8 [42]) was performed to summarize the overall effect of heat duration over time across the different communities. For no-heat control communities, measurements were used from Days 1, 3, and 5. As each community contained only one to four species, species abundances at the three time points were treated as variables (i.e., columns) and each replicate was treated as a unique observation (i.e., rows) in the abundance matrix. Distances were calculated using the Bray-Curtis dissimilarity. Heat pulse duration was fitted as an environmental vector onto the ordination using the envfit function (vegan).

Effect sizes on Shannon diversity and total productivity as compared to no-heat control were estimated in Experiment II by fitting separate generalized linear models (GLMs) for each heat duration treatment and its corresponding control on the same experiment day. For each heat duration, diversity and productivity during resistance, early recovery, and late recovery were compared to the corresponding control data from the same experiment day (e.g., days 1–3 for 6 hrs, days 3–6 for 48 hrs heat pulse; Figure 1). The full data was rescaled by its standard deviation, fitted to GLM families with different link functions (glmmTMB, version 1.1.11, [43]) that were compared by simulating their residuals (DHARMa, version 0.4.7, [44]), and the best fitting family of distributions was chosen. A lognormal or Poisson family of distributions was chosen when diversity or productivity, respectively, were used as response variables. As our data contained zero values, but the lognormal distribution does not allow zero values, we transformed the diversity data by adding a small value to all our data points ($\epsilon = \frac{\text{smallest non-zero value}}{100}$). Then, the

data was divided into four subsets for each heat duration with its corresponding no-heat control at the appropriate time points, checked for predictor multicollinearity (performance, version 0.12.4, [45]), and fitted to different models. The overall best model was selected by averaging the values of the Akaike and Bayesian information criteria (AIC and BIC, respectively) across the four data subsets. The base model had an interaction between Heat * Treatment Day. The inoculated community richness was included in the base model when the response variable was diversity and it was included in the alternative models when the response variable was productivity. Alternative models had combinations of three additional predictors: the presence of the heat resistant species *P. putida*, the presence of the strong competitor species *P. protegens*, and the expected community growth rate. The expected growth rate was estimated for each community by averaging the intrinsic growth rates of the species inoculated in that community. Effect sizes were estimated as compared to the no-heat control (effsize, version 0.8.1, [46]), then the estimated marginal means (emmeans, version 1.10.5, [47]) were used to summarize the overall effect of heat duration on resistance, early recovery, and late recovery days. For numeric non-focal predictors, this was done by using their mean values. For categorical non-focal predictors, this was done by marginalizing over the predictor levels. Finally, pairwise t-tests with a Bonferroni-correction ($\alpha = 10^{-3}$) were used to compare different heat duration treatments.

3 Results

3.1 Experiment I

3.1.1 Congeneric species exhibit consistent growth rate rankings across temperatures

We quantified the growth rate of six soil *Pseudomonas* species (in total 16 genotypes, listed in Table S1) at four temperatures, with cultures inoculated either from early exponential phase (Figure 2A) or stationary phase (Figure S4). The rank order of the species median growth rates was weakly positively correlated across temperatures (Kendall's coefficient of concordance, Wt=0.75, $\mathcal{X}^2$=11.2, df=5, p¡0.05). Except for two, most species had a consistent ranking across different temperatures.

3.1.2 Growth rates are not correlated with extreme heat resistance

To determine which of the two elevated temperatures ($35°C$ or $40°C$) constitutes a heat extreme, we assessed whether the net growth rate was substantially reduced across all species, indicating conditions severe enough to prevent cell proliferation or even induce cell mortality. Using a two-sided Wilcoxon signed rank test, we found that CFUs at $40°C$ were consistently lower than those at $35°C$ (V=$4.16 \cdot 10^3$, p< 10^{-10}), regardless of the species or growth phase of the inoculum. Figure 2B shows the CFU of cultures incubated at high temperatures relative to their CFU at the average temperature these bacteria are usually cultured at in the lab ($28°C$) for early exponential phase inocula (see Figure S5 for stationary phase inocula). Most species exhibited no growth at $40°C$ (Figure 2B). Across all species and inocula, the relative fraction of CFUs directly predicted the fraction of batch cultures with binary presence or absence of growth (all temperatures: $\beta = 0.81$, p< 10^{-10}; $40°C$: $\beta = 0.88$, p< 10^{-10}), resulting in consistent growth estimates between the batch culture data from liquid media and the CFU data from solid media (linear regression, $30°C$: $R^2 = 0.84$, F(1, 94)=508, p< 10^{-10}; $40°C$: $R^2 = 0.80$, F(1, 30)=126, p< 10^{-10}). A paired samples t-test also showed that the intrinsic growth rates were significantly lower at $40°C$ than at $35°C$ for the batch culture data (t(31)=11.5, p< 10^{-10}). Therefore, we conclude that $40°C$ can be considered sufficiently hot to be an extreme heat temperature that consistently impairs the growth of soil bacteria in our experiment.

Finally, we tested the hypothesis for Experiment I that slow growers are more resistant to extreme heat. For all analyses, we failed to reject the null hypothesis of no correlation between a species' growth rate at ambient temperatures and its ability to resist extreme heat (Tables S2-S4). There was no support for a growth rate-resistance trade-off.

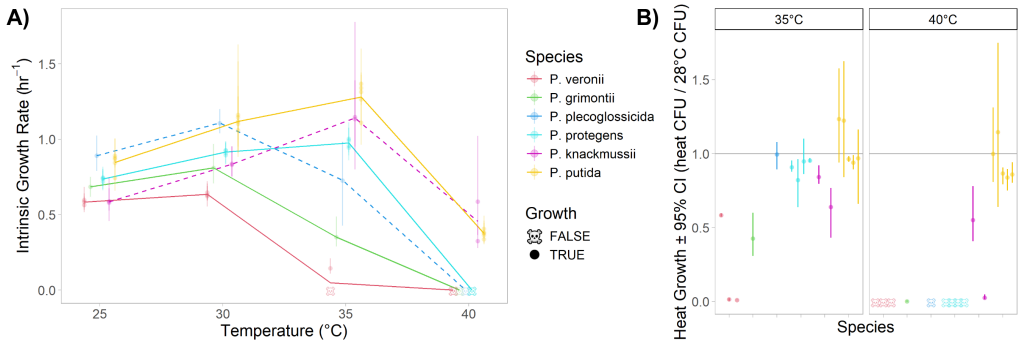

Figure 2: **Net growth rate as a function of temperature (i.e., thermal performance curves) for six bacterial species, in liquid and solid media. A)** Batch-culture intrinsic net growth rates (points) ± bootstrapped 95% confidence intervals (error bars) are shown for each strain inoculated from early exponential phase. Temperatures without consistent growth after 48hrs are shown as skulls. Lines connect species averages, with solid lines indicating species with consistent rank across temperatures (used in Experiment II) and dashed lines indicating species that change rank across temperatures. **B)** CFUs at stress temperature as a fraction of CFUs at $28°C$ (dots) ± bootstrapped 95% confidence intervals (error bars) are shown for each strain inoculated from early exponential phase. Temperatures without any growth after 7 days are shown as skulls.

3.2 Experiment II

For Experiment II, we selected four species (solid lines in Figure 2A) whose rank order is conserved across temperatures (Wt=0.90, $\mathcal{X}^2$=8.08, df=3, p¡0.05). Given that we observed no growth rate-resistance trade-off in Experiment I, we hypothesized that a conserved rank order across temperatures would lead to more predictable community responses (i.e., because the faster growing species are also more heat resistant and vice versa).

3.2.1 *P. protegens* is a strong competitor that dominates all the communities where it was inoculated

The second fastest-growing species, *P. protegens*, dominated all communities in which it was inoculated irrespective of heat treatment. This pattern is evident in the ordination plot (Figure 3A), which illustrates community trajectories over time across the resistance, early recovery, and late recovery periods (see Key Time Points in Figure 1). An NMDS with three dimensions was found to summarize much of the variation in the data (stress=0.0565; Figure S8). The ordination revealed a clear separation between communities containing *P. protegens* and those without *P. protegens*. NMDS clusters indicate a significant interaction between the presence of *P. protegens* and heat pulse duration, as confirmed by non-parametric bootstrapping (ANOSIM, R statistic = 0.621, p ¡ 0.001).

All multi-species communities inoculated with *P. protegens* lost their species richness within one day, regardless of heat (Figure 3B). The multi-species communities that were not inoculated with *P. protegens* managed to maintain at least some of their species richness over time. However, for these communities, species richness was lost as heat pulse duration increased.

We found that supernatant from *P. protegens* co-cultures has a strong inhibitory effect not seen in monoculture supernatant (Figure S9). Supernatant experiments show that *P. protegens* has inducible expression of diffusible metabolites at $30°C$ that effectively inhibit the growth of the other species (Figure 3C).

3.2.2 Fast growing communities are protected from extinction

The NMDS ordination (Figure 3A) also reveals a trend of longer heat pulse durations generally shifting community positions downward, with the exception of the longest heat pulse duration (48 hrs). This environmental gradient is not statistically significant when the 48 hr heat pulse duration

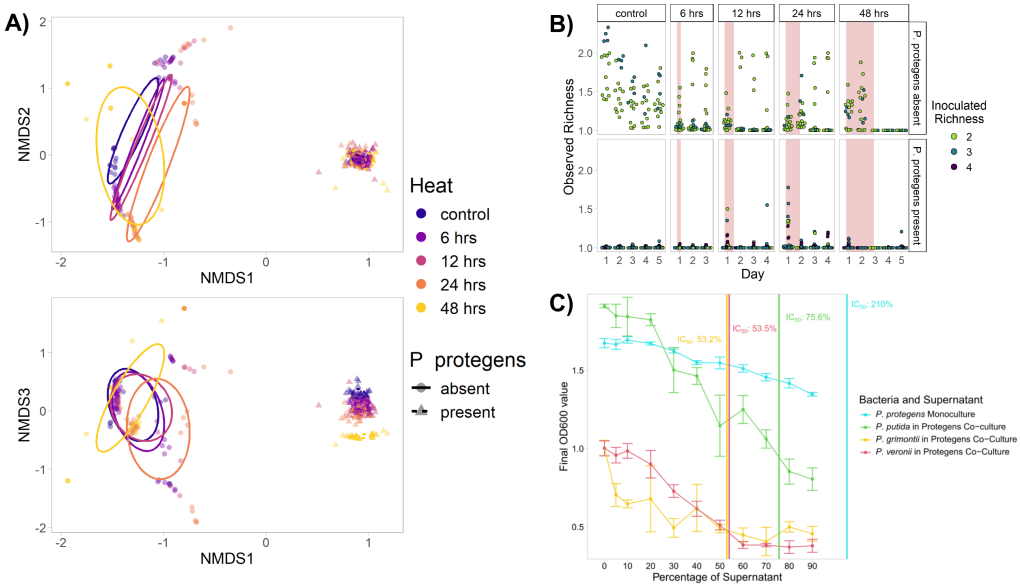

Figure 3: ***P. protegens* dominates all communities where it was inoculated because it is an effective killer. A)** Ordination plot of NMDS axes 1 versus 2 (top) and axes 1 versus 3 (bottom) shows that the presence (triangles and dashed-line ellipses) or absence (circles and solid-line ellipses) of *P. protegens* explains much of the variation in the data. The remaining variation in the data is explained by increasing heat pulse duration (warmer colours). The points show the different communities over time and the ellipses show the standard error of the (weighted) average of scores. **B) Communities without *P. protegens* (top row) and with a short duration (or no) heat pulse (left columns) maintain more of their inoculated community richness** than communities with *P. protegens* (bottom row) or with a long duration heat pulse (right columns). Points show the first-order Hill diversity index, which approximates the species richness while allowing for flow cytometry noise. The red background colour indicates days when the $40°C$ heat pulse was administered. **C) *P. protegens* expresses diffusible metabolites that effectively inhibit the growth of other bacterial species.** The presence of increasing supernatant concentration (x-axis) from *P. protegens* co-cultures has a negative effect on the final OD_{600} (y-axis). Vertical lines indicate the estimated supernatant concentration where the population's growth is inhibited by 50% (IC_{50}).

is included (p = 0.30) or when it is excluded entirely (stress = 0.0359; p = 0.22). However, the gradient becomes significant when the communities with 48 hr heat pulse but *without P. protegens* are excluded (Figure S10; stress = 0.0370; p ¡ 0.001). We noticed that communities subjected to the 48 hr heat pulse seemed more likely to go extinct, especially those without *P. protegens*.

A logistic regression model was fitted to the community extinction data (Figure S11) and it explained about 70.7% of the variation (by Efron's pseudo r-squared). The model had an additive effect of heat pulse duration, the presence of *P. protegens*, and expected community growth rate. Contrary to our hypothesis, this model was preferred over one where the presence of the heat resistant species *P. putida* was included as a predictor (ΔBIC = 48.1).

The logistic regression estimated that communities where *P. protegens* had been inoculated were less likely to go extinct. However, this estimate (odds: $2.71 \cdot 10^{-11}$, 95% CI: [0, ∞), p=0.999) is unreliable, likely because we never observed a single extinction of these communities even for the 48 hr heat pulse duration (n=35). In contrast, six communities went extinct (n=35) among those inoculated with the heat resistant *P. putida*, the species that was identified in Experiment I as growing reliably at $40°C$. If we look more closely at the growth curve data from Experiment I, we see that *P. protegens* exhibited a density-dependence in its ability to grow under extreme heat. The highest inoculum concentration at $40°C$ had a similar time to detection as for lower temperatures but all other inoculum concentrations failed to grow at this extreme heat (Figure S6). A similar result was also observed for colonies on solid media (data not shown). Unlike the other

species, *P. protegens* exhibits a positive density-dependence of growth rate even at an ambient temperature (Figure S7).

Fast-growing communities were more protected from extinction. The odds of community extinction increased by 21.5% (95% CI: [0.111, 0.319]) for each additional hour of heat pulse duration. On the other hand, communities with faster growth rates were $2.26 \cdot 10^6$ times more likely (95% CI: $[120, 4.27 \cdot 10^{10}]$) to survive for each unit of growth rate increase. In conclusion, communities with faster-growth rates and those inoculated with *P. protegens* were protected from the community extinction that was caused by longer heat pulse durations.

3.2.3 Long duration heat pulse magnifies the decoupling between resistance and recovery

To gauge how community stability changed with increasing heat pulse duration, we estimated decoupling by comparing the effect size during resistance to that during recovery for Shannon diversity and total productivity.

For diversity, the model that best fit the data was a complex model with 25 parameters: an additive effect of inoculated community richness; and a four-way interaction between the heat pulse duration, treatment day, presence of *P. protegens*, and community expected growth rate. As this model was too complex to interpret, we chose to investigate the second best model (ΔBIC = 8.32), which used the same predictors but had only 16 parameters: an additive effect of inoculated community richness; a three-way interaction between the heat pulse duration, treatment day, and presence of *P. protegens*; and an interaction between the presence of *P. protegens* and community expected growth rate. Contrary to our hypothesis, models with the presence of the heat resistant species *P. putida* fit poorly (ΔBIC $\geq$ 163). All heat pulse durations led to a significant loss of biodiversity that never recovered, even two days after the heat pulse ended (Figure S12). The loss of biodiversity was significantly greater for the 48 hr heat pulse (Table S5). The results remained consistent even after excluding extinct communities (Figure 4A). No decoupling was observed.

The model that best fit the productivity data was a complex model (26 parameters), similar to the best fitting one for biodiversity. We chose to investigate the second best model as its fit was indistinguishable (ΔBIC = 1.04). This simpler model used the same predictors but had only 16 parameters: an additive effect of community expected growth rate; a three-way interaction between the heat pulse duration, treatment day, and presence of *P. protegens*; and an interaction between presence of *P. protegens* and inoculated community richness. Contrary to our hypothesis, models with the presence of the heat resistant species *P. putida* fit poorly (ΔBIC $\geq$ 188).

We found that longer heat durations led to larger negative effects during resistance, especially for the longest heat pulse duration of 48 hrs (Figure S13, Table S6). We found that decoupling between resistance and recovery (both early and late) seemed to increase somewhat with heat duration (Figure S14). Extinct communities, by definition, were not able to recover and therefore were perfectly coupled. To assess whether the increased community extinction risk associated with longer heat pulse durations influenced our results, we excluded all communities that experienced extinction, repeated the analysis, and observed consistent results (Figure 4B). After excluding extinct communities, long heat pulse events were found to lead to slightly positive effects during recovery. A sharp increase in decoupling was observed for the 48 hr heat pulse duration (Figure 5).

4 Discussion

Our study aimed to identify the ecological mechanisms that shape soil bacterial community stability under varying heat pulse durations. We sought to predict bacterial community responses from species growth rate and heat resistance. By estimating thermal performance traits for six congeneric species (comprising 16 strains; Experiment I), we found no support for the hypothesized trade-off between growth rate and resistance. Although species exhibited consistent growth rate rankings across temperatures, these were uncorrelated with resistance to extreme heat. For the heat pulse duration experiment (Experiment II), we selected four species with variable growth rates and hypothesized that the fastest and most heat resistant species, *P. putida*, would dominate all the communities where it was inoculated. Surprisingly, an intermediate grower, *P. protegens*,

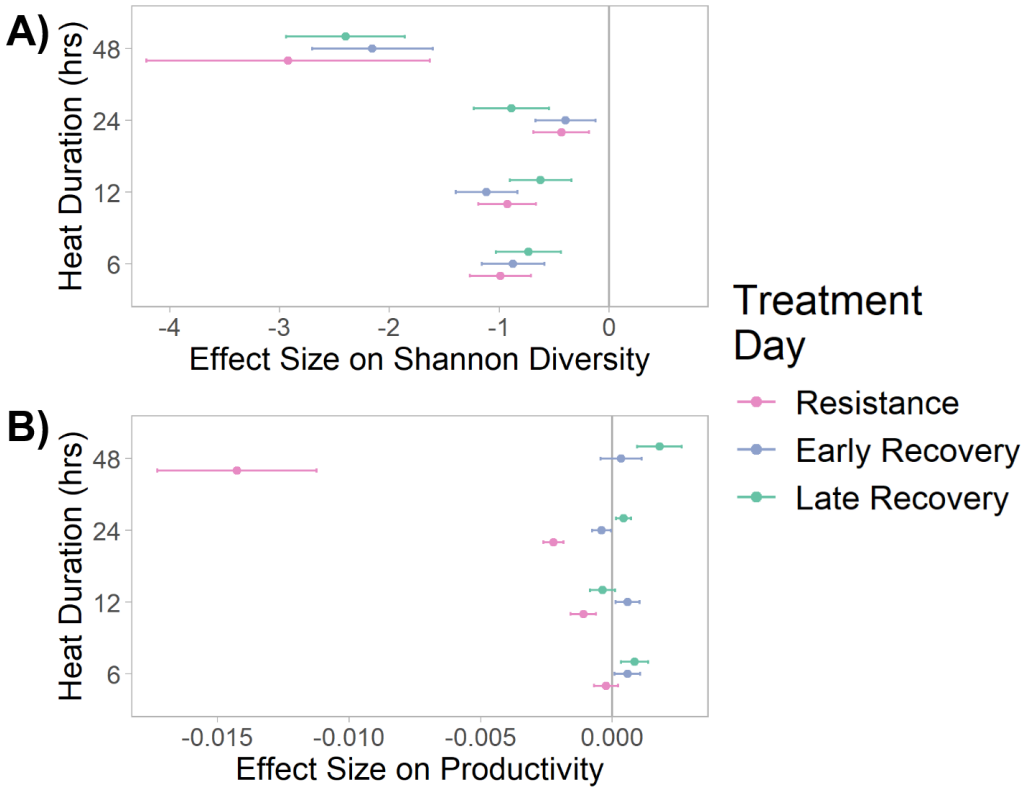

Figure 4: **Different metrics show larger effect sizes for the longest heat pulse event, 48h.** Forest plots show the estimated effect sizes and their 95% confidence intervals from generalized linear models. All communities that experienced extinction have been excluded from the data. **A)** The response variable is Shannon diversity as estimated from flow cytometry absolute cell densities for each of up to four species. **B)** The response variable is productivity as estimated from flow cytometry absolute cell density summed across all species present in the community.

out-competed all the other species, regardless of heat, because it was an effective killer. In addition, *P. protegens* was resistant to even the longest heat pulse duration, although the thermal performance screen identified it as heat sensitive.

On average, longer heat pulses drove communities to extinction. Each additional hour of heat exposure increased the odds of community extinction by 21.5%, but communities with faster growing species were substantially protected ($\sim 10^6$ times more likely to survive). Even among communities that evaded extinction, community stability decreased nonlinearly with increased heat pulse duration. Both species diversity and total productivity declined during the shorter heat pulses (6–12 hrs), then fell sharply during the longest heat pulse. The longest heat duration caused a sharp decoupling in total productivity responses during versus after the pulse, indicating reduced community stability. In summary, our study suggests that growth rates are a key factor in community stability against prolonged heatwaves. However, specific species interactions can override the predictions from monoculture traits and significantly alter the community outcomes.

4.0.1 Interspecific variation in thermal performance traits

In Experiment I, we found variation in thermal performance traits among closely related species, indicating their diverse growth strategies and heat resistances. The strains used here are primarily natural isolates but were isolated at standard culture temperatures (30 or $37°C$), so it is unclear if they accurately represent the diversity of thermal strategies adopted by soil *Pseudomonads*. Although *Pseudomonads* are broadly considered mesophiles [48], fine grain thermal niches may distinguish species. The greater between-species than within-species differences in thermal niche could suggest that this represents an important species difference in *Pseudomonads*, as previously

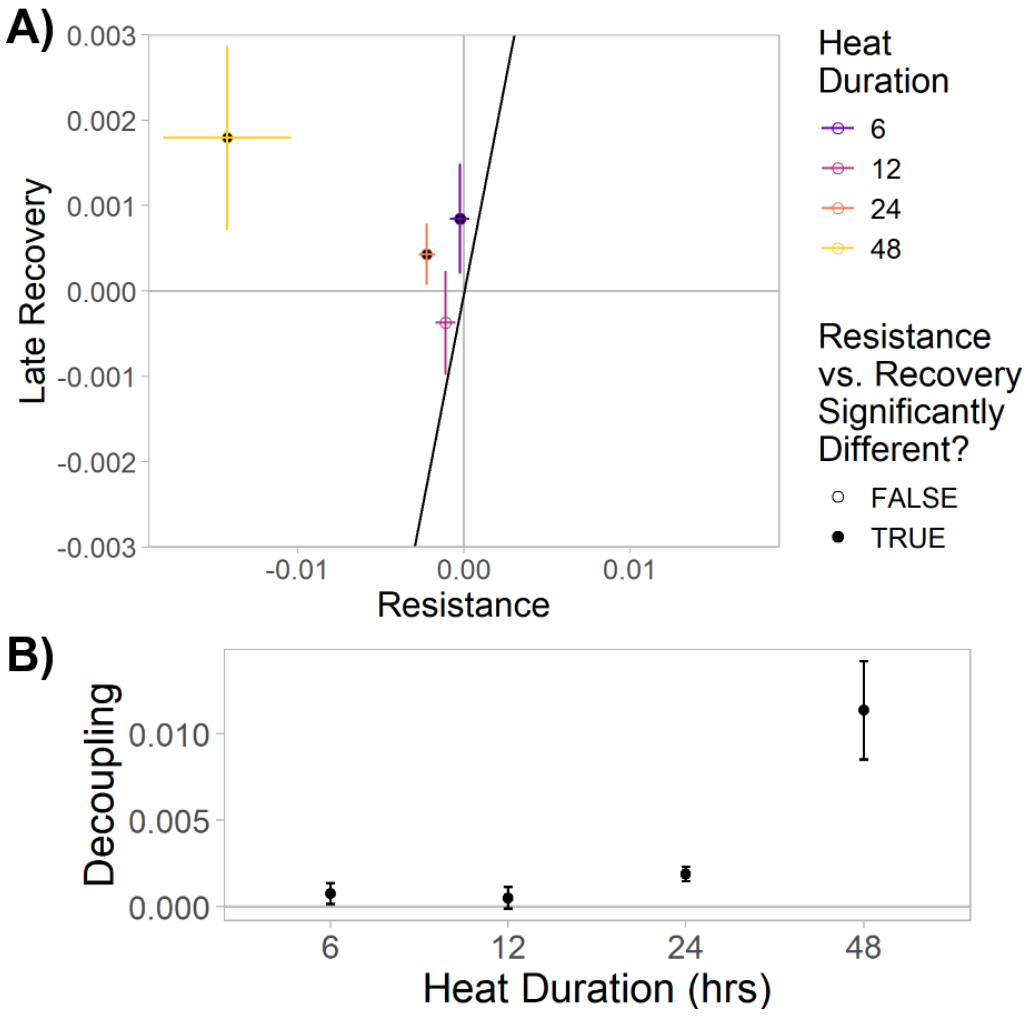

Figure 5: **Productivity exhibited decoupling of resistance from recovery, especially for the longest heat pulse duration (48h). A)** The x-axis shows the effect size on the resistance treatment day, the y-axis shows the effect size on the late recovery treatment day, and the black diagonal line indicates y=x. The coloured points show the mean estimate for different heat pulse durations and the cross-hairs indicate their univariate 95% confidence intervals. Decoupling occurs when the effect size of resistance is significantly different from that of recovery; these statistically significant points are filled with black. **B) Decoupling increases sharply for long heat pulse durations.** Mean estimated decoupling (points) is plotted directly from the panel above by measuring the shortest Euclidean distance between the point estimate and the y=x line. The lines show the confidence intervals that were estimated by drawing ovals around the univariate confidence intervals then measuring the shortest and longest Euclidean distance between the oval and the y=x line. All communities that experienced extinction have been excluded from the data.

found in Eukaryotic microbes [49]; or that the thermal niche evolves neutrally and at a slower pace than the speciation rate. The mixture of thermal niches and growth strategies observed here likely reflects the spatial and temporal heterogeneity of soil [50, 51], which supports exceptionally high microbial biodiversity [11].

4.0.2 Inter- and intra-specific interactions thwart monoculture predictions of community dynamics

Contrary to our expectation from the monoculture experiments, the intermediate grower *P. protegens* dominated all communities where it was inoculated in Experiment II and never experienced

community or species extinction. Follow-up supernatant experiments and closer examination of the growth curve OD_{600} data showed that this species is competitive because it can produce diffusible metabolites and facilitate its own growth even during extreme heat. Although the OD_{600} data at $25°C$ could be explained by cellular changes in size or aggregation, those at $40°C$ are clearly indicative of density-dependent survival or growth facilitation under stress. Our findings reinforce that monoculture-based traits, such as growth rates, cannot solely predict community dynamics, a conclusion supported by previous work [34, 52, 53]. Supernatant experiments can effectively assess species interactions but may be misleading when toxin expression is inducible [54, 55]. *P. protegens* toxicity aligns with previous studies identifying it as a biocontrol agent [56] capable of excluding other soil bacteria, including other *Pseudomonads* [57], by antibiotic secretion [58] and contact-dependent killing [59]. Future studies should investigate the mode of action of *P. protegens'* toxicity under different environmental variables relevant to climate change and in the community context [5, 9]. Finally, our work demonstrates that the time-to-detection method [33] can be used to estimate density-dependent effects. This suggests that high-throughput monoculture growth experiments can be better leveraged to estimate species functional traits [34].

4.0.3 Towards a comprehensive functional trait framework for microbial life history strategies

Our understanding of bacterial functional traits that influence life history strategies and community dynamics is limited compared to macro-biological systems. In plants, for example, functional traits such as specific leaf area, seed size, and wood density are well established as indicators of life history strategies [8]. In bacteria, the most well characterized functional trait is ribosomal RNA operon copy number, which correlates with maximum growth rate [60, 61]. However, comprehensive trait frameworks are still missing. While other studies have explored various bacterial functional traits [10, 62–64], including those related to heat resistance [16], these findings focus on distant phylogenetic relationships. Using a trait-based methodology for predicting interactions remains a challenge, especially for closely related species, as in our study. Our research suggests that density dependence in growth rate may serve as a valuable trait for predicting resistance and interactions between closely related bacteria. Future studies should systematically investigate density dependence further to determine if it correlates with life history strategies such as stress resistance and competitive ability.

4.0.4 Decoupling increases nonlinearly with heat pulse duration

The main contribution of this work is the finding that decoupling between resistance and recovery increases nonlinearly in bacterial communities due to prolonged heat pulse duration. In our study, this decoupling is driven by the positive selection of species with higher growth rate and heat resistance. The prolonged 48 hr heat pulse restructured community composition through loss of slower growing species. Communities composed of only slow-growing species were unable to recover and went extinct, exhibiting a perfect coupling between resistance and recovery. In contrast, communities that escaped extinction were enriched with fast-growing heat-resistant species, which showed over recovery. Consequently, the communities that survived extinction displayed a strong decoupling due to the intense negative response during resistance and mild positive response during recovery (Figure 5). Notably, our findings provide a new mechanism for decoupling [3] that is distinct from the trade-off between survival and fecundity that was observed for soil invertebrates exposed to heat [25]. While survival fecundity trade-offs can be identified by their positive response (high survival) during resistance and negative (low fecundity) one during recovery [25], the mechanism of decoupling that we describe here has an opposite pattern. This decoupling is caused by a positive correlation between growth rate and heat resistance in soil *Pseudomonads*, suggesting that species or stressors that elicit a growth rate-resistance trade-off may elicit different patterns of decoupling. Future studies should examine decoupling in other microbial taxa and other environmental stressors to determine if our findings are generalizable.

In contrast to a previous meta-analysis that found no evidence of a threshold effect for many types of anthropogenic global change stressors [65], our study finds nonlinear responses for prolonged heat duration. We expect this threshold effect of heat duration to be generalizable to both Eukaryotic and natural communities because it is caused by increased extinction risk with

increased heatwave duration. Extinction is a local equilibrium for most ecological systems. Future studies should look at the threshold effect of heatwave duration.

5 Conclusion

Longer heatwave durations have a nonlinear impact on bacterial communities, significantly increasing the risk of extinction for slower growing species. Even communities that avoid extinction are likely to be destabilized, as indicated by a larger decoupling between their responses during resistance and recovery. This suggests that prolonged heatwaves reshape the composition and reduce the stability of communities, particularly affecting interactions among different growth rate strategies.

Ethics. This work did not require ethical approval from a human subject or animal welfare committee.

Declaration of AI use. The writing of this manuscript was aided by use of DeepAI and ChatGPT for editorial purposes. After using these tools, the authors reviewed and revised all text as needed. We therefore assume full responsibility for the content of this document.

Conflict of interest declaration. We declare no conflict of interest.

References

[1] IPCC. 2023 Summary for Policymakers. In Core Writing Team, Lee H, Romero J, editors, *Climate change 2023: Synthesis report. Contribution of working groups I, II and III to the sixth assessment report of the Intergovernmental Panel on Climate Change* , pp. 1–34. Geneva, Switzerland.

[2] Harvey JA, Heinen R, Gols R, Thakur MP. 2020 Climate change-mediated temperature extremes and insects: from outbreaks to breakdowns. *Global change biology* **26**, 6685–6701.

[3] Martínez-De León G, Thakur MP. 2024 Ecological debts induced by heat extremes. *Trends in ecology & evolution*.

[4] Pacifici M, Foden WB, Visconti P, Watson JE, Butchart SH, Kovacs KM, Scheffers BR, Hole DG, Martin TG, Akçakaya HR et al.. 2015 Assessing species vulnerability to climate change. *Nature climate change* **5**, 215–224.

[5] de Bello F, Lavorel S, Hallett LM, Valencia E, Garnier E, Roscher C, Conti L, Galland T, Goberna M, Májeková M et al.. 2021 Functional trait effects on ecosystem stability: assembling the jigsaw puzzle. *Trends in Ecology & Evolution* **36**, 822–836.

[6] Barabás G, D'Andrea R, Stump SM. 2018 Chesson's coexistence theory. *Ecological monographs* **88**, 277–303.

[7] Lax S, Abreu CI, Gore J. 2020 Higher temperatures generically favour slower-growing bacterial species in multispecies communities. *Nature ecology & evolution* **4**, 560–567.

[8] Adler PB, Salguero-Gómez R, Compagnoni A, Hsu JS, Ray-Mukherjee J, Mbeau-Ache C, Franco M. 2014 Functional traits explain variation in plant life history strategies. *Proceedings of the National Academy of Sciences* **111**, 740–745.

[9] Stillman JH. 2019 Heat waves, the new normal: summertime temperature extremes will impact animals, ecosystems, and human communities. *Physiology* **34**, 86–100.

[10] Martiny JBH, Jones SE, Lennon JT, Martiny AC. 2015 Microbiomes in light of traits: a phylogenetic perspective. *Science* **350**, aac9323.

[11] Thompson LR, Sanders JG, McDonald D, Amir A, Ladau J, Locey KJ, Prill RJ, Tripathi A, Gibbons SM, Ackermann G et al.. 2017 A communal catalogue reveals Earth's multiscale microbial diversity. *Nature* **551**, 457–463.

[12] Whalen ED, Grandy AS, Sokol NW, Keiluweit M, Ernakovich J, Smith RG, Frey SD. 2022 Clarifying the evidence for microbial-and plant-derived soil organic matter, and the path toward a more quantitative understanding. *Global Change Biology* **28**, 7167–7185.

[13] Liang C, Schimel JP, Jastrow JD. 2017 The importance of anabolism in microbial control over soil carbon storage. *Nature microbiology* **2**, 1–6.

[14] Gilbert P, Collier PJ, Brown MR. 1990 Influence of growth rate on susceptibility to antimicrobial agents: biofilms, cell cycle, dormancy, and stringent response. *Antimicrobial agents and chemotherapy* **34**, 1865–1868.

[15] Litchman E, Edwards KF, Klausmeier CA. 2015 Microbial resource utilization traits and trade-offs: implications for community structure, functioning, and biogeochemical impacts at present and in the future. *Frontiers in microbiology* **6**, 254.

[16] Knight CG, Nicolitch O, Griffiths RI, Goodall T, Jones B, Weser C, Langridge H, Davison J, Dellavalle A, Eisenhauer N et al.. 2024 Soil microbiomes show consistent and predictable responses to extreme events. *Nature* pp. 1–7.

[17] Donohue I, Petchey OL, Montoya JM, Jackson AL, McNally L, Viana M, Healy K, Lurgi M, O'Connor NE, Emmerson MC. 2013 On the dimensionality of ecological stability. *Ecology letters* **16**, 421–429.

[18] Neubert MG, Caswell H. 1997 Alternatives to resilience for measuring the responses of ecological systems to perturbations. *Ecology* **78**, 653–665.

[19] Kéfi S, Domínguez-García V, Donohue I, Fontaine C, Thébault E, Dakos V. 2019 Advancing our understanding of ecological stability. *Ecology letters* **22**, 1349–1356.

[20] Hillebrand H, Langenheder S, Lebret K, Lindström E, Östman Ö, Striebel M. 2018 Decomposing multiple dimensions of stability in global change experiments. *Ecology letters* **21**, 21–30.

[21] Ochoa-Hueso R, Delgado-Baquerizo M, Risch AC, Schrama M, Morriën E, Barmentlo SH, Geisen S, Hannula SE, Resch MC, Snoek BL et al.. 2021 Ecosystem coupling: A unifying framework to understand the functioning and recovery of ecosystems. *One Earth* **4**, 951–966.

[22] Bender EA, Case TJ, Gilpin ME. 1984 Perturbation experiments in community ecology: theory and practice. *Ecology* **65**, 1–13.

[23] Moreno-Mateos D, Alberdi A, Morriën E, van der Putten WH, Rodríguez-Uña A, Montoya D. 2020 The long-term restoration of ecosystem complexity. *Nature Ecology & Evolution* **4**, 676–685.

[24] Thakur MP, Risch AC, van der Putten WH. 2022 Biotic responses to climate extremes in terrestrial ecosystems. *Iscience* **25**.

[25] Martínez-De León G, Marty A, Holmstrup M, Thakur MP. 2024 Population resistance and recovery after an extreme heat event are explained by thermal effects on life-history traits. *Oikos* **2024**, e10023.

[26] Isbell F, Craven D, Connolly J, Loreau M, Schmid B, Beierkuhnlein C, Bezemer TM, Bonin C, Bruelheide H, De Luca E et al.. 2015 Biodiversity increases the resistance of ecosystem productivity to climate extremes. *Nature* **526**, 574–577.

[27] Tohya M, Teramoto K, Watanabe S, Hishinuma T, Shimojima M, Ogawa M, Tada T, Tabe Y, Kirikae T. 2022 Whole-genome sequencing-based re-identification of Pseudomonas putida/fluorescens clinical isolates identified by biochemical bacterial identification systems. *Microbiology Spectrum* **10**, e02491–21.

[28] Sentchilo VS, Perebituk AN, Zehnder AJ, van der Meer JR. 2000 Molecular diversity of plasmids bearing genes that encode toluene and xylene metabolism in Pseudomonas strains isolated from different contaminated sites in Belarus. *Applied and environmental microbiology* **66**, 2842–2852.

[29] Howell C, Stipanovic R. 1979 Control of Rhizoctonia solani on cotton seedlings with Pseudomonas fluorescens and with an antibiotic produced by the bacterium. *Phytopathology* **69**, 480–482.

[30] Batsch M, Guex I, Todorov H, Heiman CM, Vacheron J, Vorholt JA, Keel C, van der Meer JR. 2024 Fragmented micro-growth habitats present opportunities for alternative competitive outcomes. *Nature communications* **15**, 7591.

[31] Péchy-Tarr M, Borel N, Kupferschmied P, Turner V, Binggeli O, Radovanovic D, Maurhofer M, Keel C. 2013 Control and host-dependent activation of insect toxin expression in a root-associated biocontrol pseudomonad. *Environmental microbiology* **15**, 736–750.

[32] Schlechter RO, Jun H, Bernach M, Oso S, Boyd E, Muñoz-Lintz DA, Dobson RC, Remus DM, Remus-Emsermann MN. 2018 Chromatic bacteria–A broad host-range plasmid and chromosomal insertion toolbox for fluorescent protein expression in bacteria. *Frontiers in Microbiology* **9**, 3052.

[33] Mytilinaios I, Salih M, Schofield HK, Lambert RJ. 2012 Growth curve prediction from optical density data. *International journal of food microbiology* **154**, 169–176.

[34] Ghenu AH, Marrec L, Bank C. 2024 Challenges and pitfalls of inferring microbial growth rates from lab cultures. *Frontiers in Ecology and Evolution* **11**, 1313500.

[35] Chen CY, Nace GW, Irwin PL. 2003 A 6× 6 drop plate method for simultaneous colony counting and MPN enumeration of Campylobacter jejuni, Listeria monocytogenes, and Escherichia coli. *Journal of microbiological methods* **55**, 475–479.

[36] Hall BG, Acar H, Nandipati A, Barlow M. 2014 Growth rates made easy. *Molecular biology and evolution* **31**, 232–238.

[37] Mansoury M, Hamed M, Karmustaji R, Al Hannan F, Safrany ST. 2021 The edge effect: A global problem. The trouble with culturing cells in 96-well plates. *Biochemistry and biophysics reports* **26**, 100987.

[38] Elzhov TV, Mullen KM, Spiess AN, Bolker B. 2023 *minpack.lm: R Interface to the Levenberg-Marquardt Nonlinear Least-Squares Algorithm Found in MINPACK, Plus Support for Bounds (version 1.2-4)*. DOI: 10.32614/CRAN.package.minpack.lm.

[39] R Core Team. 2024 *R: A Language and Environment for Statistical Computing*. R Foundation for Statistical Computing Vienna, Austria.

[40] Mira P, Yeh P, Hall BG. 2022 Estimating microbial population data from optical density. *Plos one* **17**, e0276040.

[41] Blazanin M. 2024 gcplyr: an R package for microbial growth curve data analysis. *BMC bioinformatics* **25**, 232.

[42] Oksanen J, Simpson GL, Blanchet FG, Kindt R, Legendre P, Minchin PR, O'Hara R, Solymos P, Stevens MHH, Szoecs E, Wagner H, Barbour M, Bedward M, Bolker B, Borcard D, Carvalho G, Chirico M, De Caceres M, Durand S, Evangelista HBA, FitzJohn R, Friendly M, Furneaux B, Hannigan G, Hill MO, Lahti L, McGlinn D, Ouellette MH, Ribeiro Cunha E, Smith T, Stier A, Ter Braak CJ, Weedon J, Borman T. 2025 *vegan: Community Ecology Package*. DOI: 10.32614/CRAN.package.vegan.

[43] McGillycuddy M, Warton DI, Popovic G, Bolker BM. 2025 Parsimoniously Fitting Large Multivariate Random Effects in glmmTMB. *Journal of Statistical Software* **112**, 1–19. (10.18637/jss.v112.i01)

[44] Hartig F. 2024 *DHARMa: Residual Diagnostics for Hierarchical (Multi-Level / Mixed) Regression Models*. DOI: 10.32614/CRAN.package.DHARMa.

[45] Lüdecke D, Ben-Shachar MS, Patil I, Waggoner P, Makowski D. 2021 performance: An R Package for Assessment, Comparison and Testing of Statistical Models. *Journal of Open Source Software* **6**, 3139. (10.21105/joss.03139)

[46] Torchiano M. 2020 *effsize: Efficient Effect Size Computation.* DOI: 10.32614/CRAN.package.effsize.

[47] Lenth RV. 2025 *emmeans: Estimated Marginal Means, aka Least-Squares Means.* DOI: 10.32614/CRAN.package.emmeans.

[48] Andreani NA, Fasolato L. 2017 *Pseudomonas* and related genera. In *The microbiological quality of food* , pp. 25–59. Elsevier.

[49] Mozzachiodi S, Bai FY, Baldrian P, Bell G, Boundy-Mills K, Buzzini P, Čadež N, Cubillos FA, Dashko S, Dimitrov R et al.. 2022 Yeasts from temperate forests. *Yeast* **39**, 4–24.

[50] Zeigler DR. 2014 The Geobacillus paradox: why is a thermophilic bacterial genus so prevalent on a mesophilic planet?. *Microbiology* **160**, 1–11.

[51] Upton RN, Bach EM, Hofmockel KS. 2019 Spatio-temporal microbial community dynamics within soil aggregates. *Soil Biology and Biochemistry* **132**, 58–68.

[52] Concepción-Acevedo J, Weiss HN, Chaudhry WN, Levin BR. 2015 Malthusian parameters as estimators of the fitness of microbes: a cautionary tale about the low side of high throughput. *PloS one* **10**, e0126915.

[53] Balsa-Canto E, Alonso-del Real J, Querol A. 2020 Mixed growth curve data do not suffice to fully characterize the dynamics of mixed cultures. *Proceedings of the National Academy of Sciences* **117**, 811–813.

[54] Dedrick S, Warrier V, Lemon KP, Momeni B. 2023 When does a Lotka-Volterra model represent microbial interactions? Insights from in vitro nasal bacterial communities. *Msystems* **8**, e00757–22.

[55] Schmitz DA, Wechsler T, Mignot I, Kümmerli R. 2024 Predicting bacterial interaction outcomes from monoculture growth and supernatant assays. *ISME communications* **4**, ycae045.

[56] Ramette A, Frapolli M, Fischer-Le Saux M, Gruffaz C, Meyer JM, Défago G, Sutra L, Moënne-Loccoz Y. 2011 Pseudomonas protegens sp. nov., widespread plant-protecting bacteria producing the biocontrol compounds 2, 4-diacetylphloroglucinol and pyoluteorin. *Systematic and applied microbiology* **34**, 180–188.

[57] Vick SH, Fabian BK, Dawson CJ, Foster C, Asher A, Hassan KA, Midgley DJ, Paulsen IT, Tetu SG. 2021 Delving into defence: identifying the Pseudomonas protegens Pf-5 gene suite involved in defence against secreted products of fungal, oomycete and bacterial rhizosphere competitors. *Microbial Genomics* **7**, 000671.

[58] Zhang Q, Kong X, Li S, Chen XJ, Chen XJ. 2020 Antibiotics of Pseudomonas protegens FD6 are essential for biocontrol activity. *Australasian plant pathology* **49**, 307–317.

[59] Vacheron J, Péchy-Tarr M, Brochet S, Heiman CM, Stojiljkovic M, Maurhofer M, Keel C. 2019 T6SS contributes to gut microbiome invasion and killing of an herbivorous pest insect by plant-beneficial Pseudomonas protegens. *The ISME journal* **13**, 1318–1329.

[60] Klappenbach JA, Dunbar JM, Schmidt TM. 2000 rRNA operon copy number reflects ecological strategies of bacteria. *Applied and environmental microbiology* **66**, 1328–1333.

[61] Roller BR, Stoddard SF, Schmidt TM. 2016 Exploiting rRNA operon copy number to investigate bacterial reproductive strategies. *Nature microbiology* **1**, 1–7.

[62] Louca S, Parfrey LW, Doebeli M. 2016 Decoupling function and taxonomy in the global ocean microbiome. *Science* **353**, 1272–1277.

[63] Madin JS, Nielsen DA, Brbic M, Corkrey R, Danko D, Edwards K, Engqvist MK, Fierer N, Geoghegan JL, Gillings M et al.. 2020 A synthesis of bacterial and archaeal phenotypic trait data. *Scientific data* **7**, 170.

[64] Cébron A, Zeghal E, Usseglio-Polatera P, Meyer A, Bauda P, Lemmel F, Leyval C, Maunoury-Danger F. 2021 BactoTraits–A functional trait database to evaluate how natural and man-induced changes influence the assembly of bacterial communities. *Ecological Indicators* **130**, 108047.

[65] Hillebrand H, Donohue I, Harpole WS, Hodapp D, Kucera M, Lewandowska AM, Merder J, Montoya JM, Freund JA. 2020 Thresholds for ecological responses to global change do not emerge from empirical data. *Nature Ecology & Evolution* **4**, 1502–1509.

Supplement for: Longer heatwaves disrupt bacterial communities by decoupling resistance from recovery.

[Authors temporarily removed for peer review]

Materials & Methods

Table S1: List of bacterial strains used in the experiment.

ID	Strain identification	Isolated from…	Fluorescence	Lab of Origin & Strain ID in their Collection	Ref.
BSC001	*Pseudomonas putida F1*	creek	sYFP	Jan van der Meer (UniL, CH) 7609	--
BSC002	*Pseudomonas putida KT2440*	?	mScarlet	Jan van der Meer (UniL, CH) 7598	--
BSC003	*Pseudomonas putida uwc 2*	soil	mTagBFP2	Jan van der Meer (UniL, CH) 7597	--
BSC004	*Pseudomonas veronii*	?	mTagBFP2	Jan van der Meer (UniL, CH) 7591	--
BSC005	*Pseudomonas veronii*	?	mScarlet	Jan van der Meer (UniL, CH) 7592	--
BSC006	*Pseudomonas veronii*	?	mCherry	Jan van der Meer (UniL, CH) 3434	--
BSC007	*Pseudomonas knackmussii B13*	soil	mCherry	Jan van der Meer (UniL, CH) 2586	--
BSC008	*Pseudomonas knackmussii B14*	sewage	eGFP	Jan van der Meer (UniL, CH) 1369	--
BSC009	*Pseudomonas plecoglossicida*	soil	*N/A*	Antonis Chatzinotas (UFZ, DE) B405	[30]
BSC010	*Pseudomonas putida mt-2 KT2440*	soil	*N/A*	Antonis Chatzinotas (UFZ, DE) B410	--
BSC015	*Pseudomonas putida KT2440*	?	GFP	Pilar Junier (UniNe, CH)	--
BSC019	*Pseudomonas grimontii*	soil	*N/A*	Jan van der Meer (UniL, CH) 906 (SV16)	[31]
CK101	*Pseudomonas protegens Pf5*	soil	mTourquoise2	Christof Keel (UniL, CH) Pf5-*mtou*	[32]
CK102	*Pseudomonas protegens Pf5*	soil	mCherry	Christof Keel (UniL, CH) Pf5-*mche*	[33]
CK103	*Pseudomonas protegens CHAO*	soil	sGFP2	Christof Keel (UniL, CH) CHA0-*gfp2*	[34]
CK104	*Pseudomonas protegens CHAO*	soil	mCherry	Christof Keel (UniL, CH) CHA0-*mche*	[34]
BSC028	*Pseudomonas grimontii*	*(see above)*	sGFP2	**BSC019**	This.

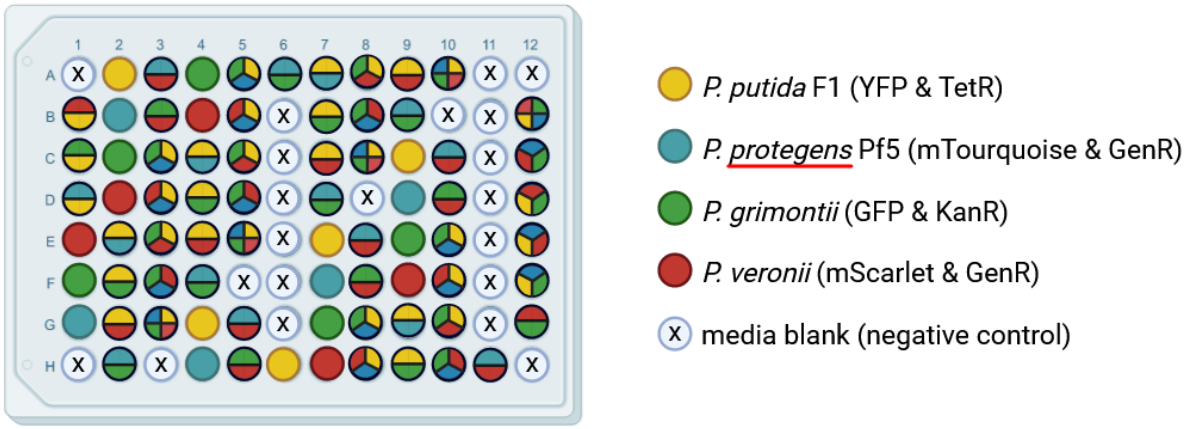

Figure S1. The arrangement of the 15 communities (n=5) on the 96-well microplates during Experiment II. Communities are arranged in five blocks across the microplate such that two of the blocks are all edge wells and the other three blocks are all non-edge wells. Coloured circles represent communities inoculated with the species indicated in the legend. Media blanks are shown with crosses. Figure created with BioRender.

Figure S2. Flow cytometry gating strategy to identify individual species. All events in the cells gate **(panel A)** are either assigned to species level, using a set of three nested polygon gates to identify events with single fluorophore expression **(panels B-E)**, or excluded from further analyses. For panels B-E), representative screenshots are taken from the FCS Express analysis for a positive sample (top plots) with all four species present and a negative sample (bottom plots) with the three other species present.

A)

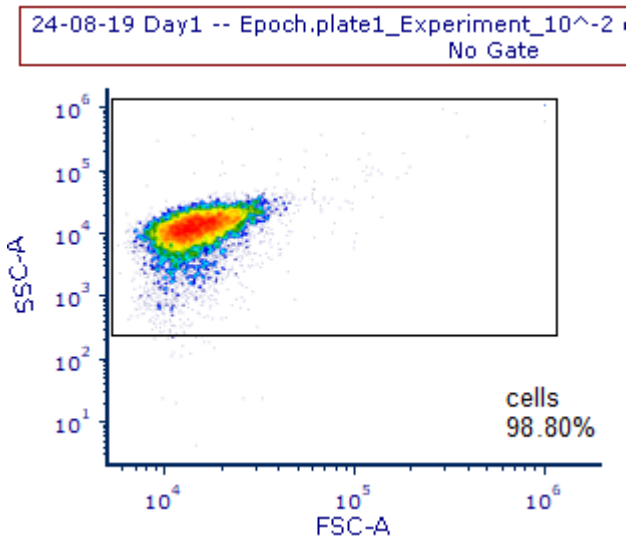

Figure S2 Panel A) A rectangular gate (black) in the forward scatter area (FSC-A) and side scatter area (SSC-A) was used to identify cells and exclude small particles, which are most likely debris.

B)

Gating strategy to identify the YFP-positive cell population (*P. putida)*:

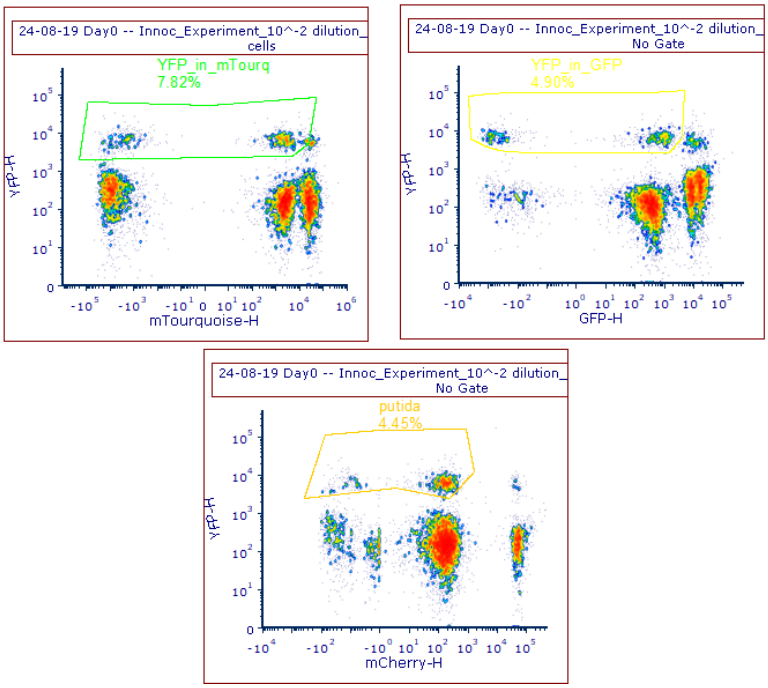

The same strategy for a sample without *P. putida* (YFP-negative):

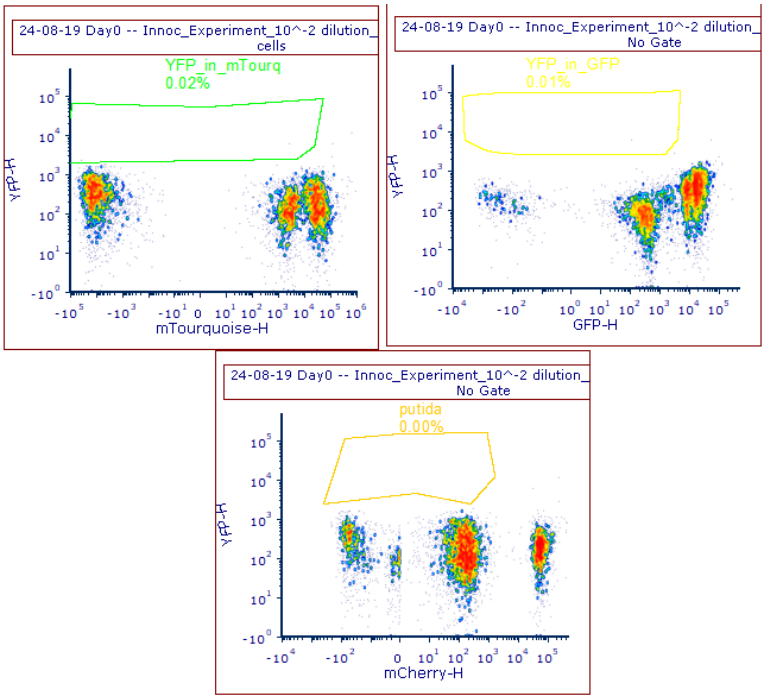

Figure S2 Panel B) Events from the cells gate are assigned to *P. putida* species because they express only YFP, as measured in YFP height (YFP-H, y-axis of all plots). First, mTourquoise events are excluded using a polygon gate in mTourquoise height (mTourquoise-H), then GFP events are excluded using a polygon gate in GFP height (GFP-H), and finally mCherry events are excluded using a polygon gate in mCherry height (mCherry-H).

C)

Gating strategy to identify the mTourquoise-positive cell population (*P. protegens)*:

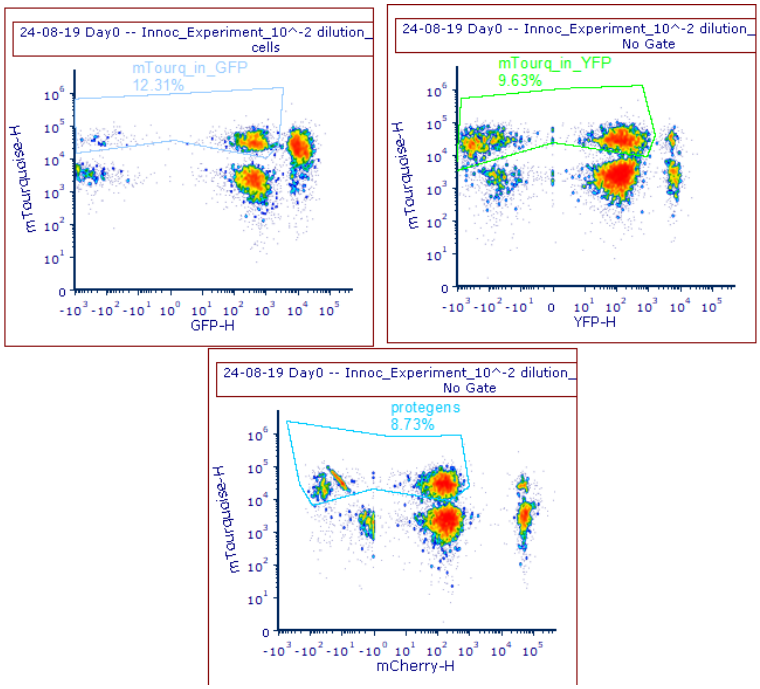

The same strategy for a sample without *P. protegens* (mTourquoise-negative):

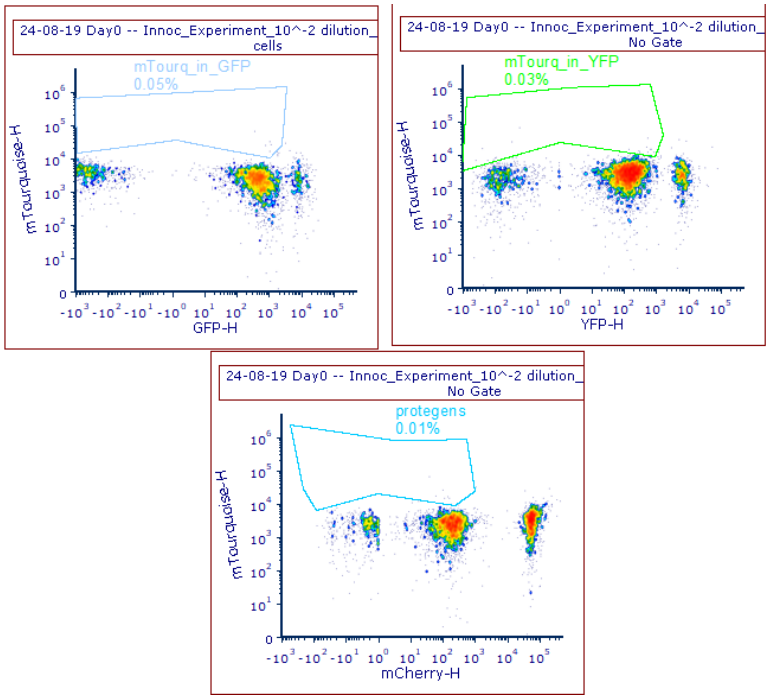

Figure S2 Panel C) Events from the cells gate are assigned to *P. protegens* species because they express only mTourquoise, as measured in mTourquoise height (mTourquoise-H, y-axis of all plots). First, GFP events are excluded using a polygon gate in GFP height (GFP-H), then YFP events are excluded using a polygon gate in YFP height (YFP-H), and finally mCherry events are excluded using a polygon gate in mCherry height (mCherry-H).

D)

Gating strategy to identify the GFP-positive cell population (*P. grimontii)*:

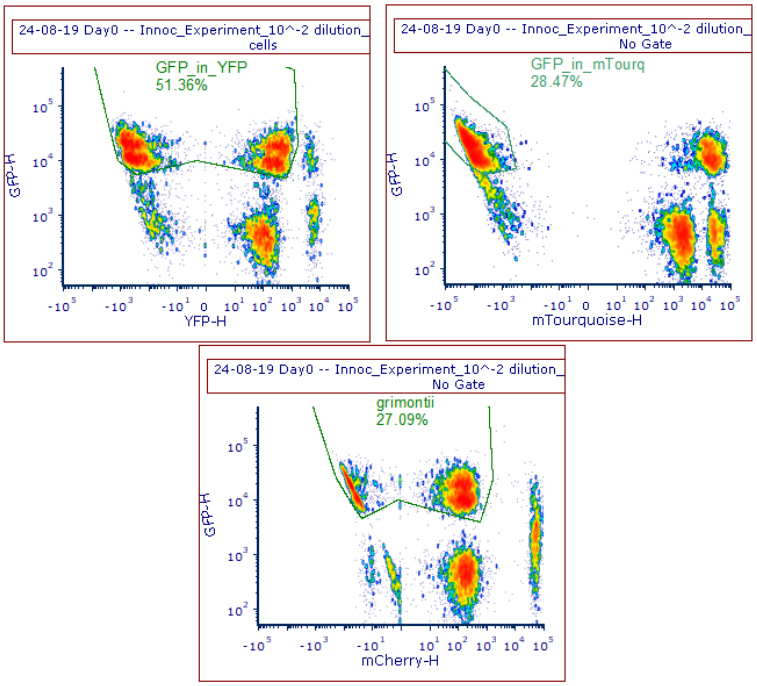

The same strategy for a sample without *P. grimontii* (GFP-negative):

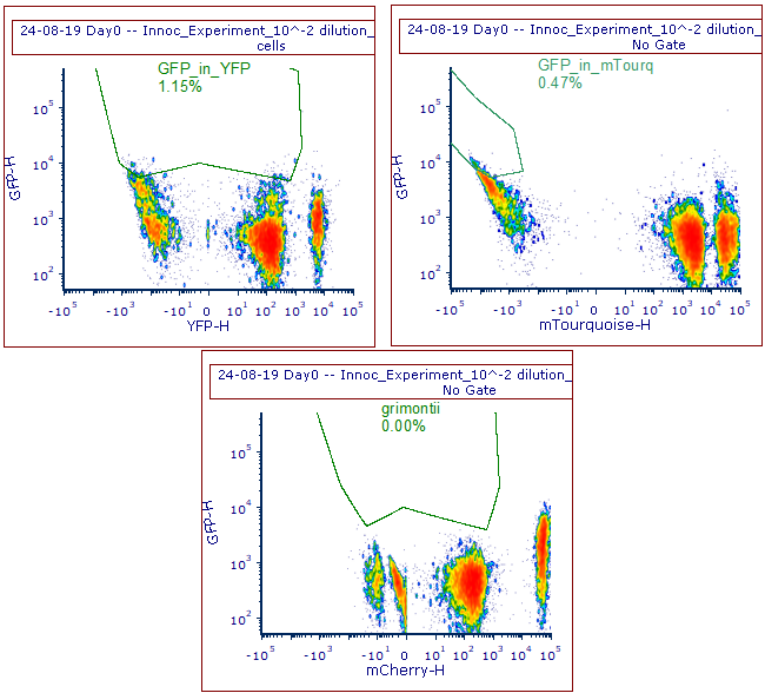

Figure S2 Panel D) Events from the cells gate are assigned to *P. grimontii* species because they express only GFP, as measured in GFP height (GFP-H, y-axis of all plots). First, YFP events are excluded using a polygon gate in YFP height (YFP-H), then mTourquoise events are excluded using a polygon gate in mTourquoise height (mTourquoise-H), and finally mCherry events are excluded using a polygon gate in mCherry height (mCherry-H).

E)

Gating strategy to identify the mCherry-positive cell population (*P. veronii)*:

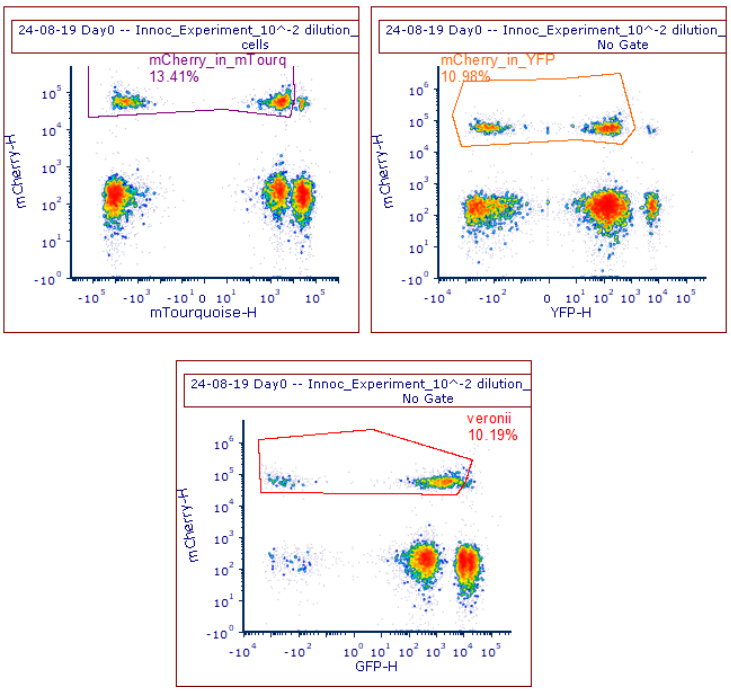

The same strategy for a sample without *P. veronii* (mCherry-negative):

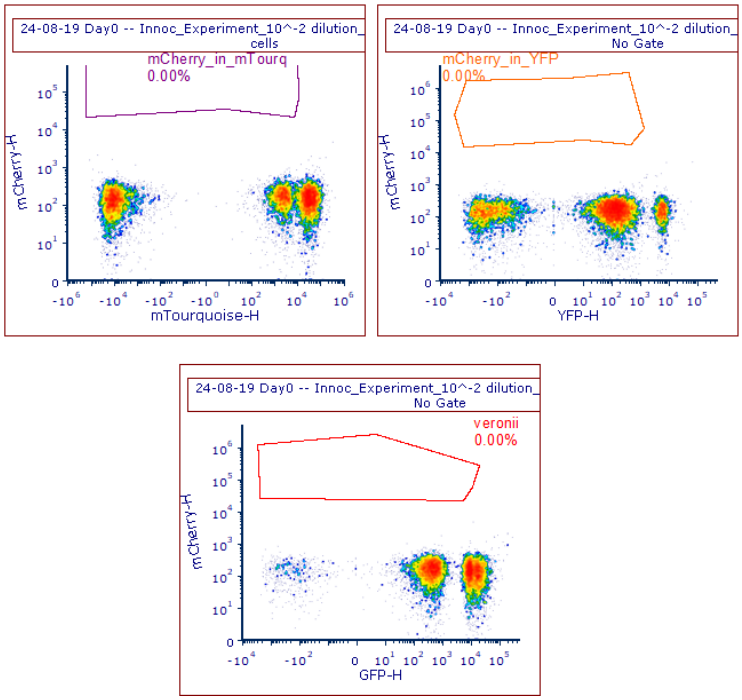

Figure S2 Panel E) Events from the cells gate are assigned to *P. veronii* species because they express only mCherry, as measured in mCherry height (mCherry-H, y-axis of all plots). First, mTourquoise events are excluded using a polygon gate in mTourquoise height (mTourquoise-H), then YFP events are excluded using a polygon gate in YFP height (YFP-H), and finally GFP events are excluded using a polygon gate in GFP height (GFP-H).

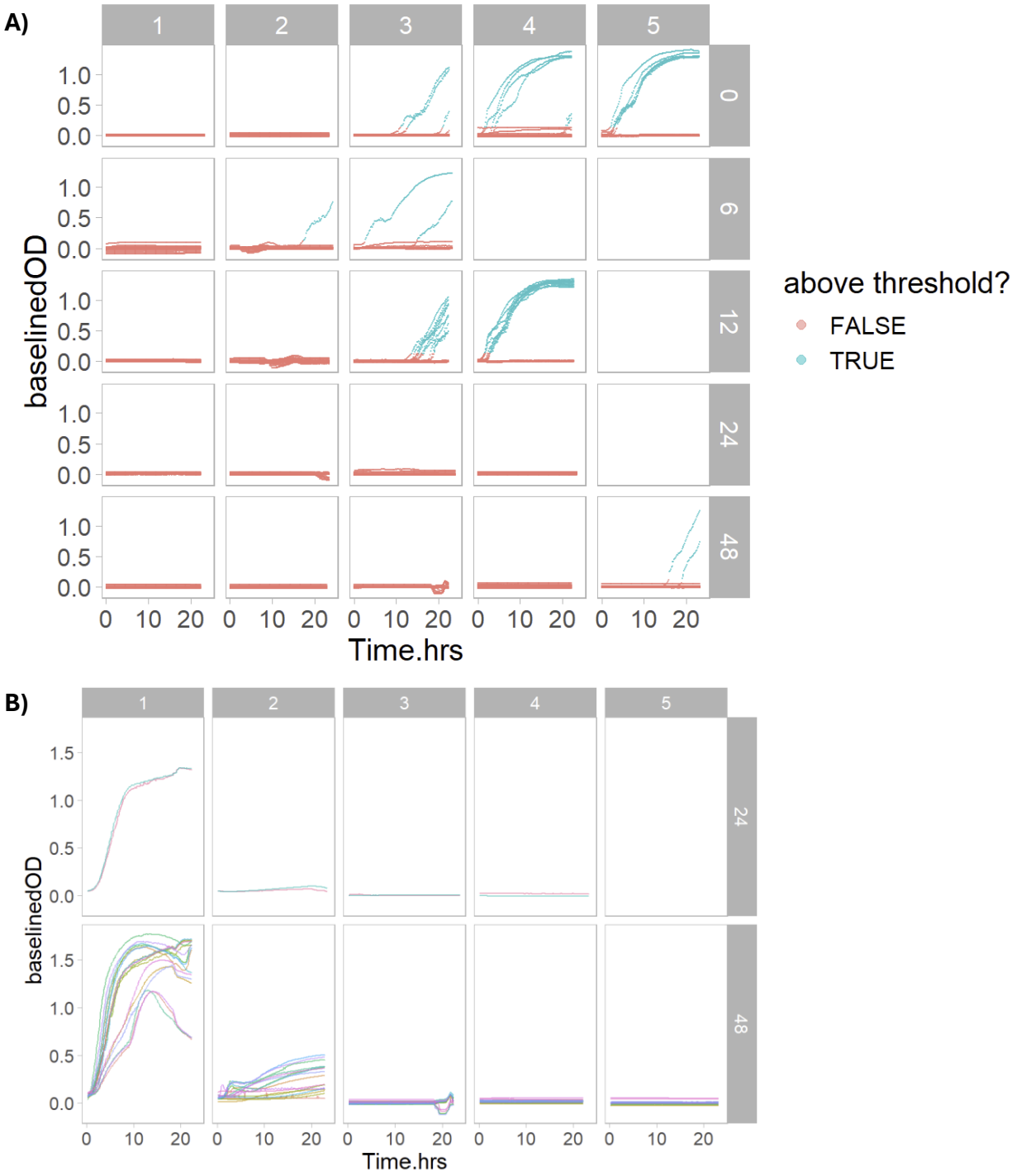

Figure S3. The same threshold was used for identifying contaminated well blanks (A) and wells that experienced community extinction (B). Different columns indicate the day of growth (Day 1 to 5) and different rows indicate the duration of the heat pulse treatment (0 indicates no heat control, 6 hrs heat, 12 hrs heat, 24 hrs heat, or 48 hrs heat) as illustrated in Figure 1 of the main text. There is no data for Days 4-5 of 6 hrs heat and Day 5 for 12 & 24 hrs heat (see main text). **A) Shows the baseline-subtracted OD for all well blanks, including contaminated well blanks.** Datapoints that are above the threshold are shown in blue and indicate contaminated blank wells. **B) Shows the baseline-subtracted OD only for non-blank communities that went extinct.** Datapoints are coloured by unique replicates.

Results for Experiment I

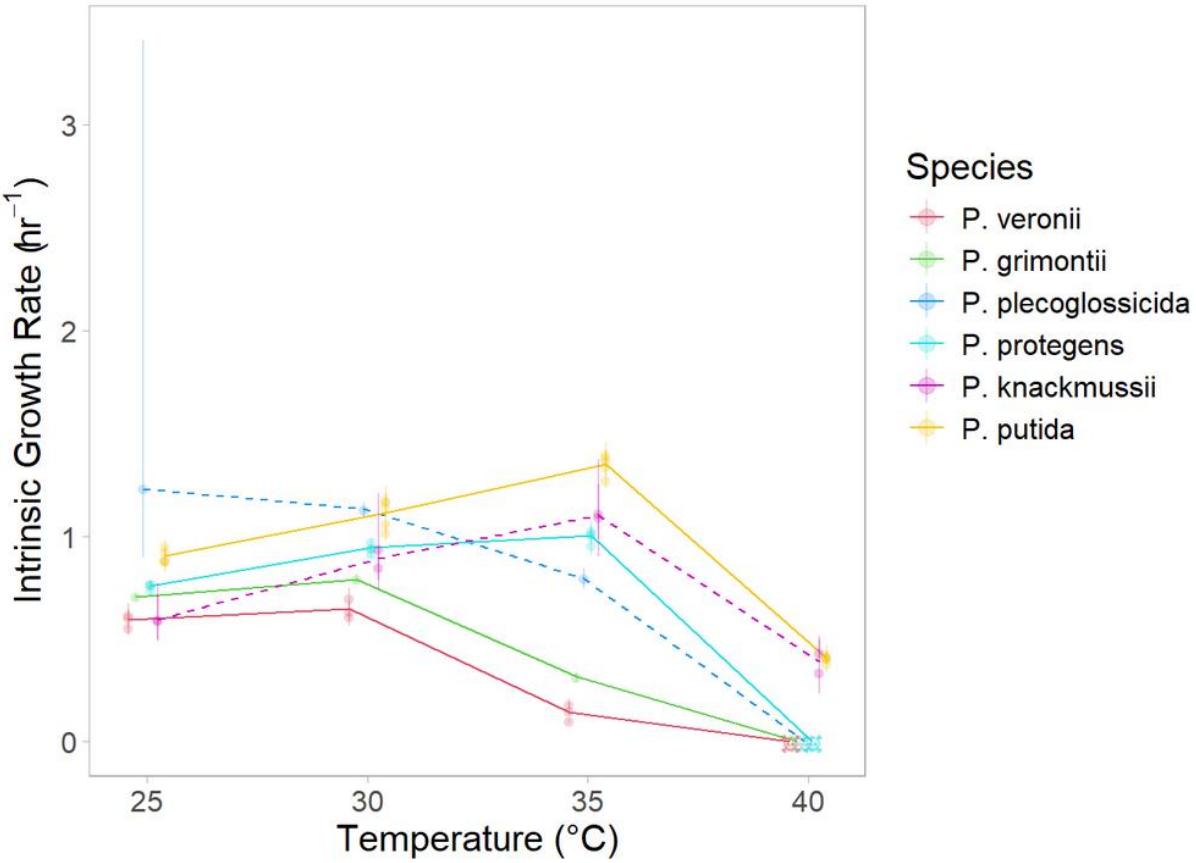

Figure S4. Net growth rate of stationary phase cultures as a function of temperature for 6 bacterial species in liquid media. Batch-culture intrinsic net growth rates (points) ± bootstrapped 95% confidence intervals (error bars) are shown for each strain inoculated from stationary phase. Temperatures without consistent growth after 48hrs are shown as skulls. Lines connect species averages, with solid lines indicating species with consistent rank across temperatures (used in Experiment II) and dashed lines indicating species that change rank across temperatures.

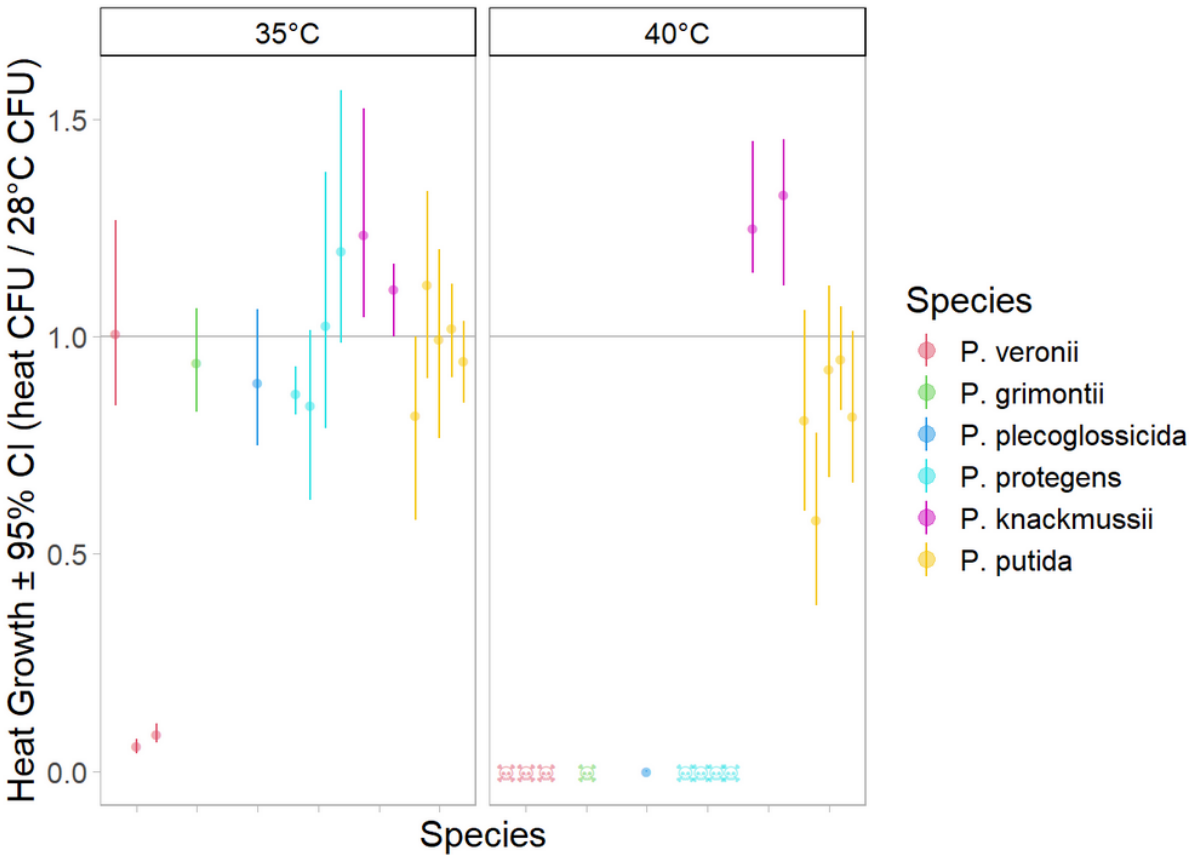

Figure S5. Relative growth of stationary phase cultures as a function of temperature for 6 bacterial species in solid media. CFUs at stress temperature as a fraction of CFUs at 28°C (dots) ± bootstrapped 95% confidence intervals (error bars) are shown for each strain inoculated from early exponential phase. Temperatures without any growth after 7 days are shown as skulls.

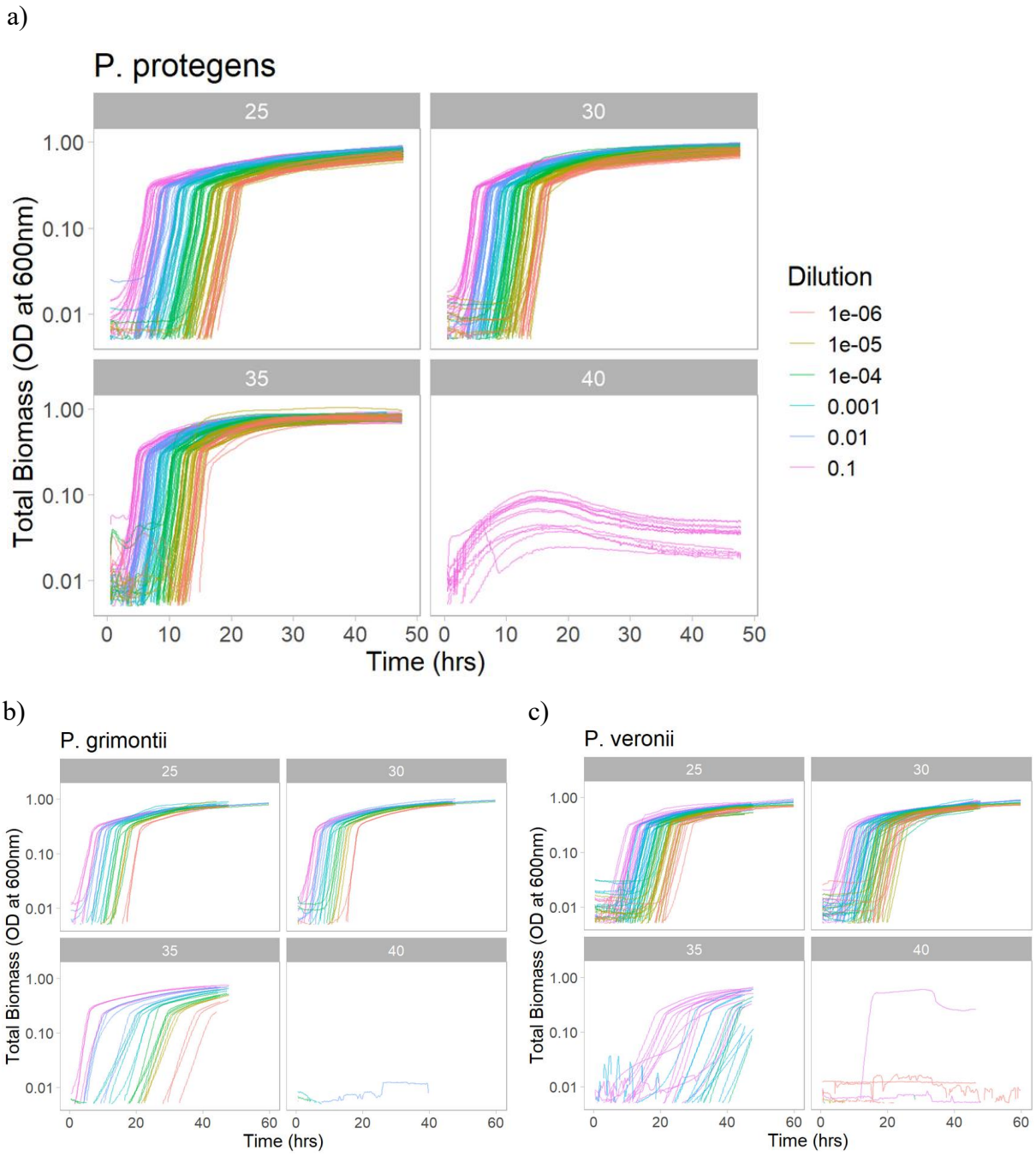

Figure S6. *P. protegens* (a) exhibits density-dependence during growth at extreme heat, but other species that are also sensitive to extreme heat, *P. grimontii* (b) and *P. veronii* (c), do not show density-dependent growth. Each panel shows the log of the OD (y-axis) over time (x-axis) for batch cultures inoculated, from both early exponential and stationary phase, at different starting dilutions (colours) that were incubated at different temperatures (facets). The most concentrated *P. protegens* cultures grew at about the same rate in the first five hours of growth at 40°C as when those was incubated at lower temperatures. However, there was a complete absence of growth at 40°C for all other starting concentrations.

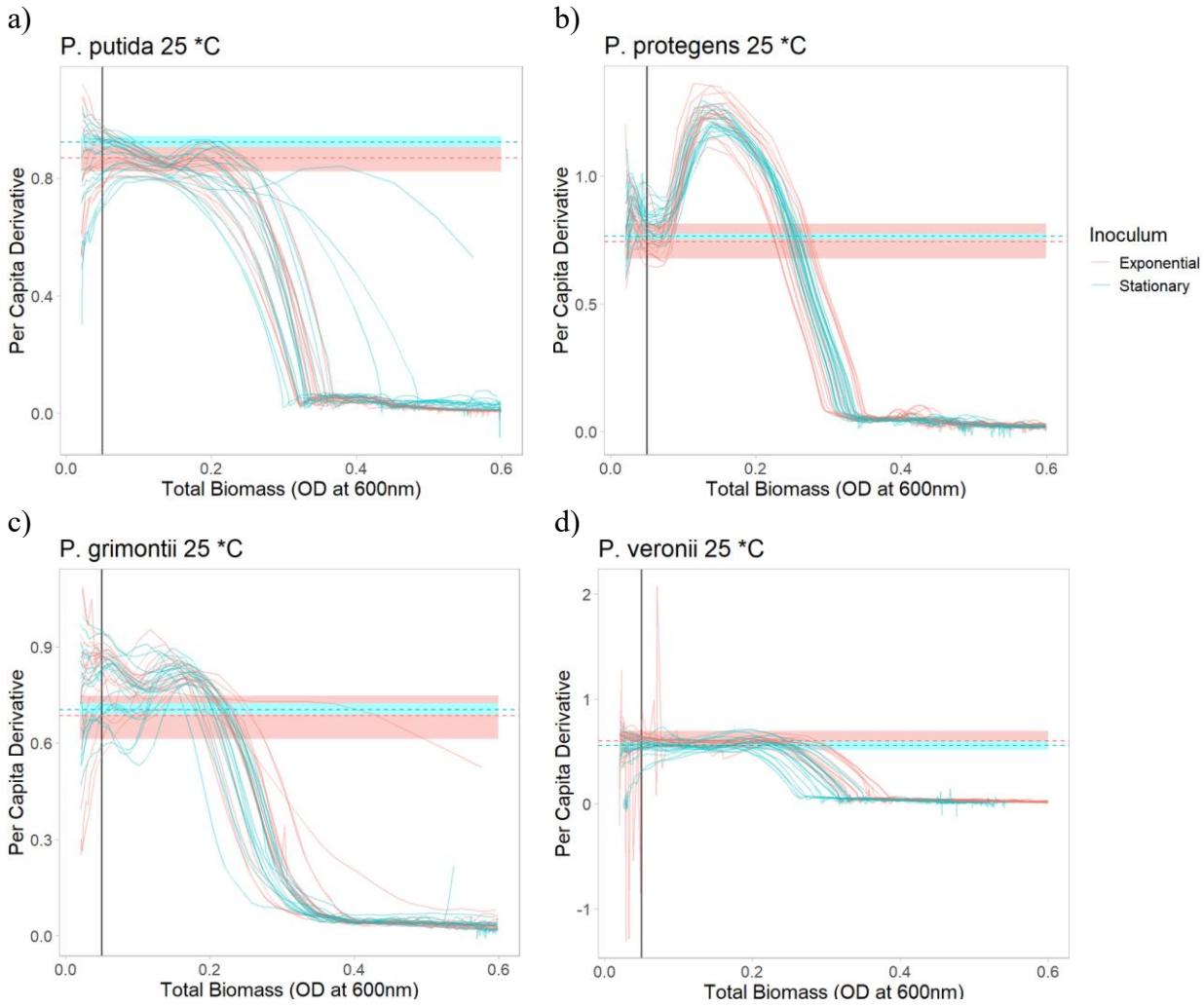

Figure S7. *P. protegens* (b) exhibits a consistent and strong density-dependence of growth rate at 25°C, as compared to other species (a, c, d). Each panel shows the per capita derivative of OD (y-axis) as a function of OD (x-axis) at 25°C for batch cultures inoculated at different starting dilutions from either early exponential (red) or stationary (blue) phase. The horizontal dashed lines show the mean of the intrinsic growth rate, coloured by exponential or stationary phase estimate, and the ribbons show the corresponding 95% confidence intervals. The black vertical line shows the threshold of detection that was used to estimate the intrinsic growth rate. By convention, the intrinsic growth rate (μ) is defined as the growth rate in the absence of density-dependent effects. For all species, the intrinsic growth rate estimates are in good agreement with the per capita derivatives at low density (i.e., near the black line). **b)** *P. protegens* cultures show a consistent ~50% increase in the per capita derivative of OD at intermediate OD (~0.15) as compared to low OD. This could suggest that *P. protegens* cells can facilitate each other's growth more than other species.

Table S2. Non-parametric tests of whether intrinsic growth rate rank at ambient temperatures is correlated with that at extreme heat (Spearman's rank correlation).

Correlation of species rank at 25°C with that at 40°C		
rho = -0.34	S = 46.8	p-value = 0.51

Correlation of species rank at 30°C with that at 40°C		
rho = 0.30	S = 24.4	p-value = 0.56

Table S3. Parametric tests of whether intrinsic growth rate at ambient temperatures is correlated with that at extreme heat (linear mixed effects model).

lm(intrinsic growth rate at 40°C ~ intrinsic growth rate at 25°C + (1 | Species))			
Efron R^2 = 0.962			
	Estimate	SE	p-value
Fixed effects			
Intercept	0.084	0.13	0.52 (NS)
Growth at 25°C	0.068	0.14	0.63 (NS)
Random effect			
Species (intercept)	0.037	0.19	

lm(intrinsic growth rate at 40°C ~ intrinsic growth rate at 30°C + (1 | Species))			
Efron R^2 = 0.962			
	Estimate	SE	p-value
Fixed effects			
Intercept	0.21	0.20	0.28 (NS)
Growth at 30°C	-0.086	0.20	0.67 (NS)
Random effect			
Species (intercept)	0.038	0.19	

Table S4. Parametric test of whether intrinsic growth rate at ambient temperatures is correlated with the relative growth by CFU (linear mixed effects model).
Bonferroni-corrected α = 0.025

lm(relative growth by CFU at 40°C ~ intrinsic growth rate at 25°C + (1 | Species))			
Efron R^2 = 0.81			
	Estimate	SE	p-value
Fixed effects			
Intercept	0.26	0.49	0.59 (NS)
Growth at 25°C	0.034	0.60	0.96 (NS)
Random effect			
Species (intercept)	0.15	0.38	

lm(relative growth by CFU at 40°C ~ intrinsic growth rate at 30°C + (1 | Species))			
Efron R^2 = 0.83			
	Estimate	SE	p-value
Fixed effects			
Intercept	-0.98	0.66	0.14 (NS)
Growth at 30°C	1.4	0.70	0.048 (NS)
Random effect			
Species (intercept)	0.13	0.36	

Results for Experiment II

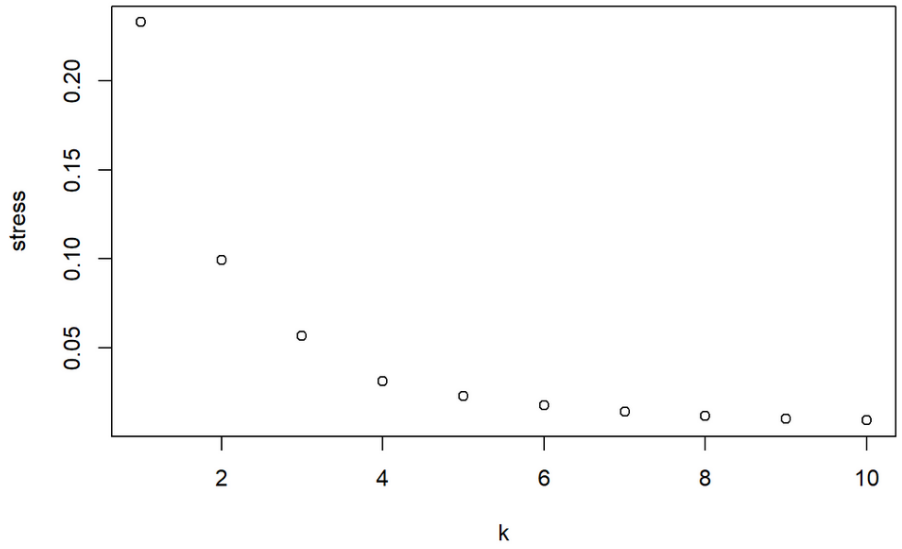

Figure S8. Scree plot of NMDS ordination for all communities over time on the resistance, early recovery, and late recovery days. Three dimensions were used for the analysis as the this is dimensionality is readily interpretable and the decrease in stress plateaus off around k=3.

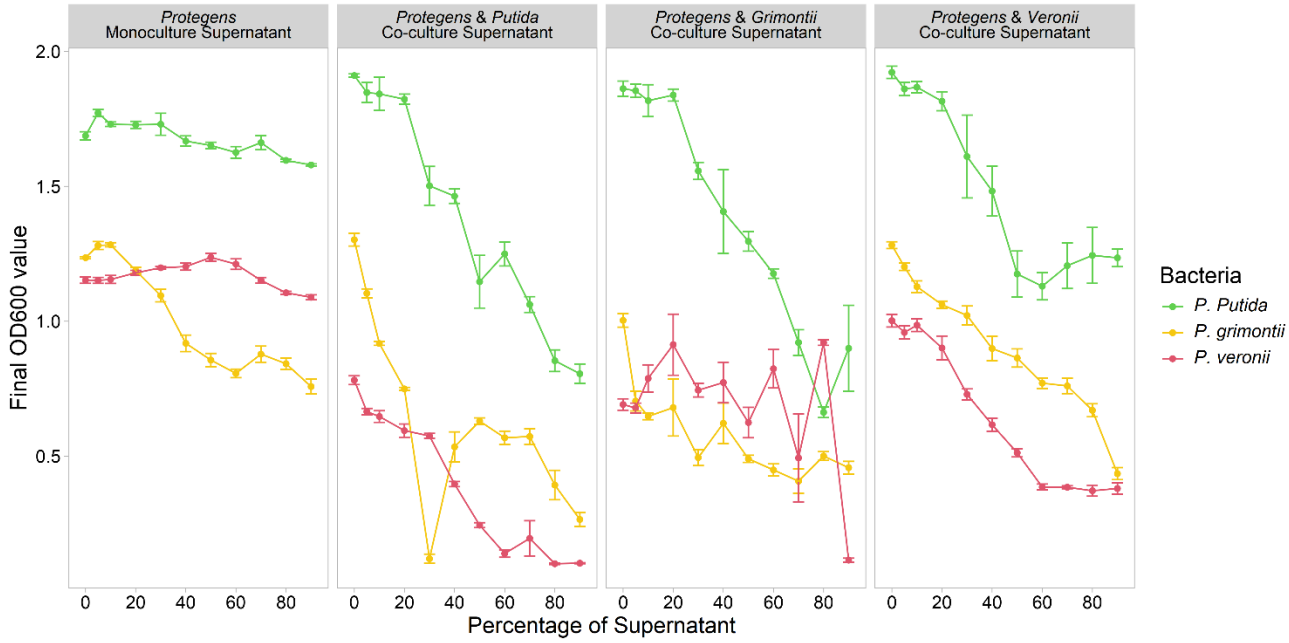

Figure S9. Average OD values for three of the focal species after 12 hours of growth versus percentage of media that is supernatant (compared to fresh 50% LB). This figure is the same style and is part of the motivation for Figure 3C. Here we compare the growth of these bacterial species when subjected to *P. protegens* supernatant when *P. protegens* is grown alone versus when *P. protegens* is grown with another species.

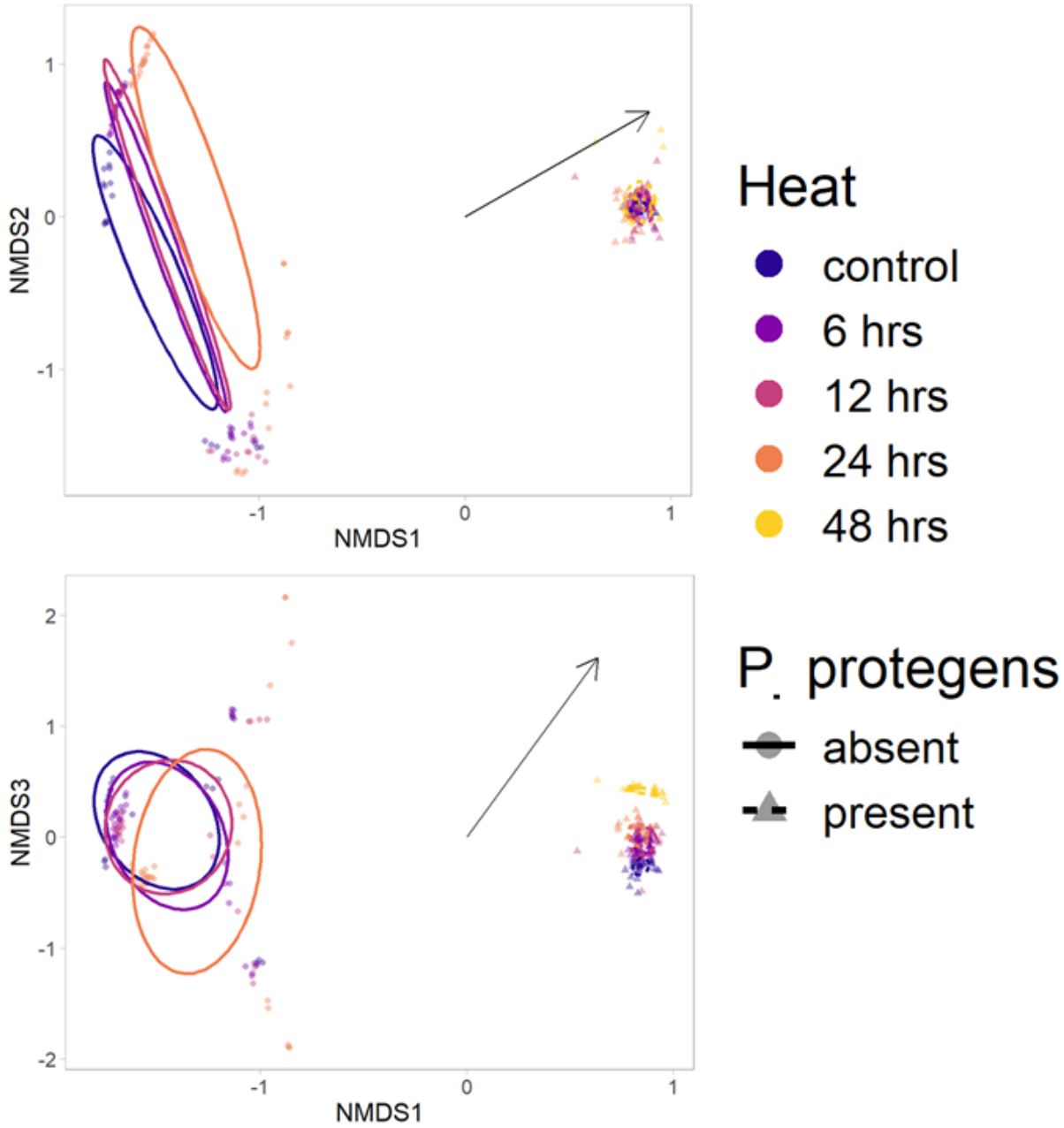

Figure S10. NMDS ordination for the data excluding the communities without *P. protegens* that were exposed to 48h heat pulse duration. The figure style is the same as Figure 3A from the main text except for the thin black arrows. The arrows show the direction of the environmental gradient of heat pulse duration (which is statistically significant, $p<0.001$).

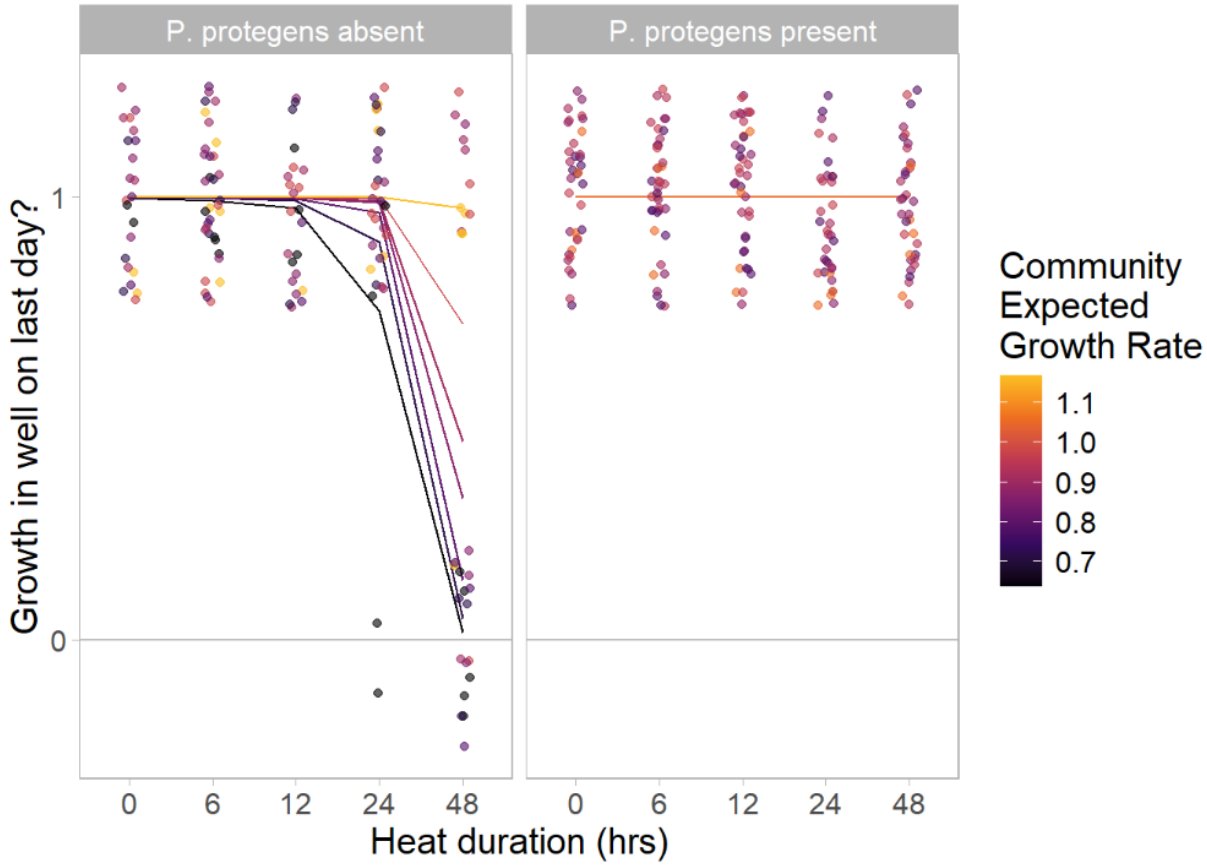

Figure S11. Logistic regression found three risk factors for community extinction: the duration of the heat pulse, the absence of *P. protegens* from the community, and slow community expected growth rate. Points show the observed data and lines show the logistic model predictions. Heat duration was treated as a numeric variable in the model although it is shown here on the x-axis as a categorical variable. The y-axis is binary and indicates whether growth was observed in the well two days after the end of the heat pulse (i.e., the final day of the experiment). Colours show the community expected growth rates, and the facets show communities without (left) and with (right) *P. protegens*. Multiple identical model predictions are stacked on top of one another in the right facet.

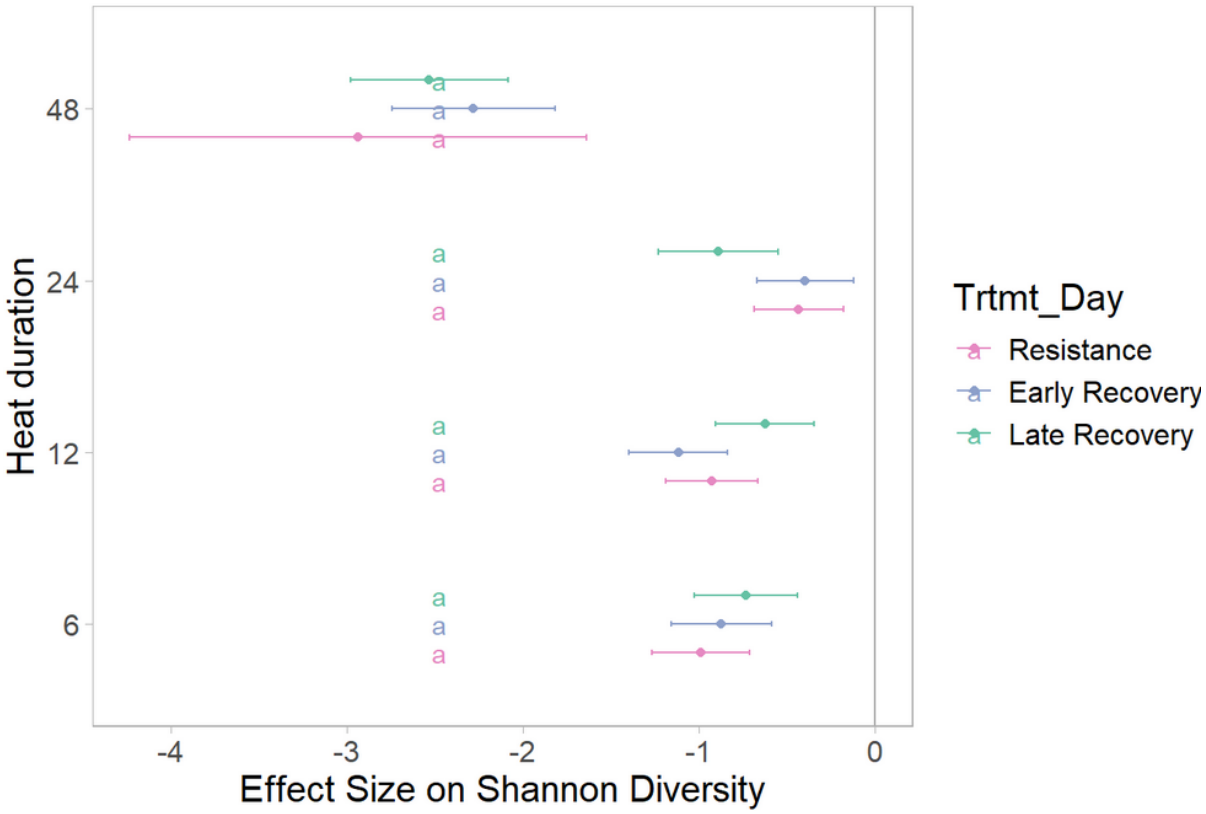

Figure S12. Forest plot of the effect sizes on Shannon diversity for the complete data (i.e., *including* communities that went extinct). The figure style is the same as Figure 4A from the main text. The colours indicate different treatment days and the letters indicate treatment days *within the same heat pulse duration* that are statistically indistinguishable.

Table S5. Pairwise t-tests between heat pulse durations on the effect sizes of Shannon diversity for the complete data (i.e., *including* communities that went extinct).
Bonferroni-corrected α = 0.001

Treatment Day	1st Heat Pulse Duration	Compared to 2nd Heat Pulse Duration	t-statistic	df	p-value	Adjusted p-value	
Resistance	6 hrs	12 hrs	-1.17	24.2	0.253	1.00	NS
		24 hrs	-10.3	23.2	$p < 10^{-9}$	$p < 10^{-6}$	*
		48 hrs	9.79	11.3	$p < 10^{-6}$	$p < 10^{-4}$	*
	12 hrs	24 hrs	-9.25	22.5	$p < 10^{-6}$	$p < 10^{-6}$	*
		48 hrs	10.1	11.3	$p < 10^{-6}$	$p < 10^{-4}$	*
	24 hrs	48 hrs	12.6	11.3	$p < 10^{-6}$	$p < 10^{-6}$	*
Early Recovery	6 hrs	12 hrs	4.32	24.2	$p < 10^{-3}$	0.00418	NS
		24 hrs	-8.38	23.0	$p < 10^{-6}$	$p < 10^{-6}$	*
		48 hrs	17.5	16.8	$p < 10^{-9}$	$p < 10^{-9}$	*
	12 hrs	24 hrs	-12.6	22.4	$p < 10^{-9}$	$p < 10^{-9}$	*
		48 hrs	14.5	16.9	$p < 10^{-9}$	$p < 10^{-6}$	*
	24 hrs	48 hrs	23.3	17.0	$p < 10^{-12}$	$p < 10^{-12}$	*
Late Recovery	6 hrs	12 hrs	-1.93	24.2	0.0655	1.00	NS
		24 hrs	2.37	21.5	0.0274	0.493	NS
		48 hrs	22.8	17.7	$p < 10^{-12}$	$p < 10^{-12}$	*
	12 hrs	24 hrs	4.10	20.9	$p < 10^{-3}$	0.00932	NS
		48 hrs	24.4	17.3	$p < 10^{-12}$	$p < 10^{-12}$	*
	24 hrs	48 hrs	19.5	19.6	$p < 10^{-12}$	$p < 10^{-12}$	*

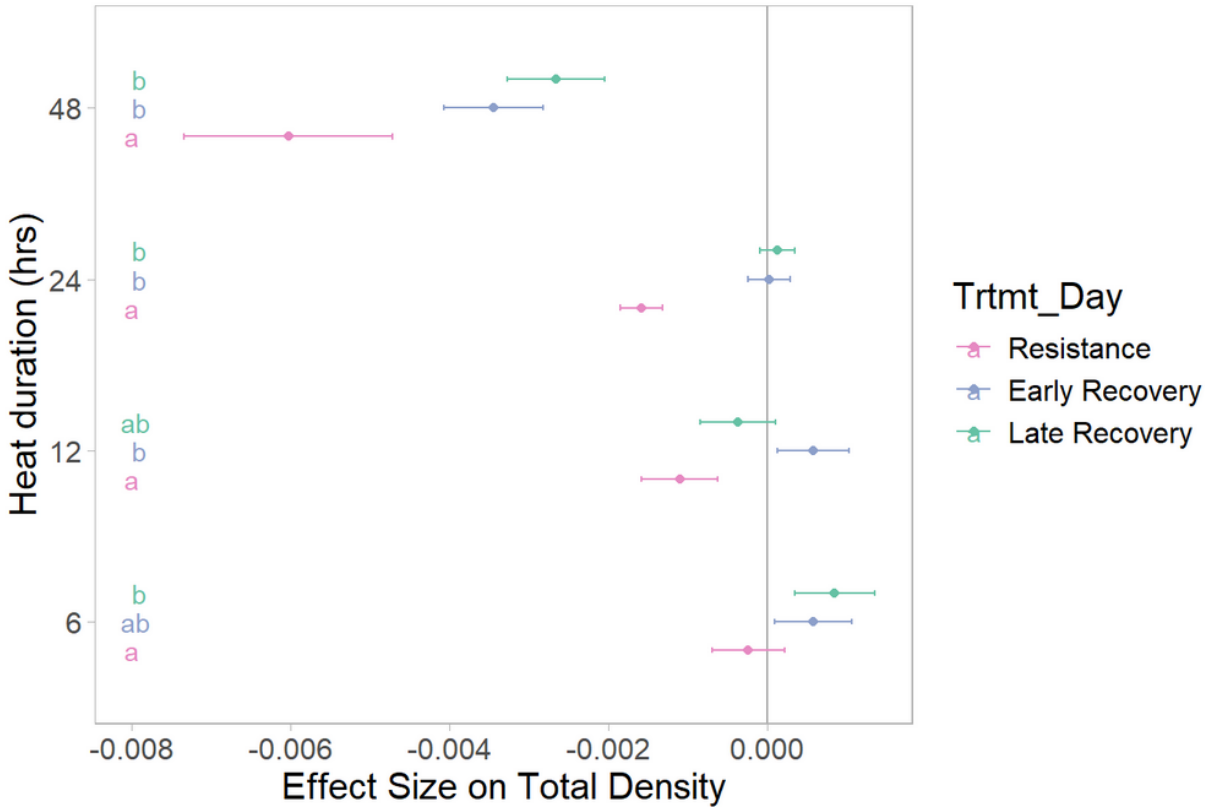

Figure S13. Forest plot of the effect sizes on productivity for the complete data (i.e., including communities that were never able to recover because they went extinct). The figure style is the same as Figure 4B from the main text. The colours indicate different treatment days and the letters indicate groups of treatment days *within the same heat pulse duration* that are statistically indistinguishable.

Table S6. Pairwise t-tests between heat pulse durations on the effect sizes of total productivity for the complete data (i.e., *including* communities that went extinct). Bonferroni-corrected α = 0.001

Treatment Day	1st Heat Pulse Duration	Compared to 2nd Heat Pulse Duration	t-statistic	df	p-value	Adjusted p-value	
Resistance	6 hrs	12 hrs	10.5	30.8	$p < 10^{-9}$	$p < 10^{-9}$	*
		24 hrs	21.2	28.5	$p < 10^{-18}$	$p < 10^{-15}$	*
		48 hrs	32.9	18.1	$p < 10^{-15}$	$p < 10^{-15}$	*
	12 hrs	24 hrs	6.86	22.6	$p < 10^{-6}$	$p < 10^{-4}$	*
		48 hrs	27.6	19.0	$p < 10^{-15}$	$p < 10^{-12}$	*
	24 hrs	48 hrs	26.1	16.2	$p < 10^{-12}$	$p < 10^{-12}$	*
Early Recovery	6 hrs	12 hrs	-0.0725	32.0	0.943	1.00	NS
		24 hrs	8.27	27.6	$p < 10^{-6}$	$p < 10^{-6}$	*
		48 hrs	40.9	28.9	$p < 10^{-18}$	$p < 10^{-18}$	*
	12 hrs	24 hrs	8.34	23.6	$p < 10^{-6}$	$p < 10^{-6}$	*
		48 hrs	40.9	27.3	$p < 10^{-18}$	$p < 10^{-18}$	*
	24 hrs	48 hrs	40.3	20.1	$p < 10^{-18}$	$p < 10^{-18}$	*
Late Recovery	6 hrs	12 hrs	14.2	31.9	$p < 10^{-12}$	$p < 10^{-12}$	*
		24 hrs	10.9	24.2	$p < 10^{-9}$	$p < 10^{-6}$	*
		48 hrs	35.6	29.3	$p < 10^{-18}$	$p < 10^{-18}$	*
	12 hrs	24 hrs	-7.44	20.3	$p < 10^{-6}$	$p < 10^{-4}$	*
		48 hrs	23.0	28.3	$p < 10^{-18}$	$p < 10^{-18}$	*
	24 hrs	48 hrs	33.8	18.6	$p < 10^{-15}$	$p < 10^{-15}$	*

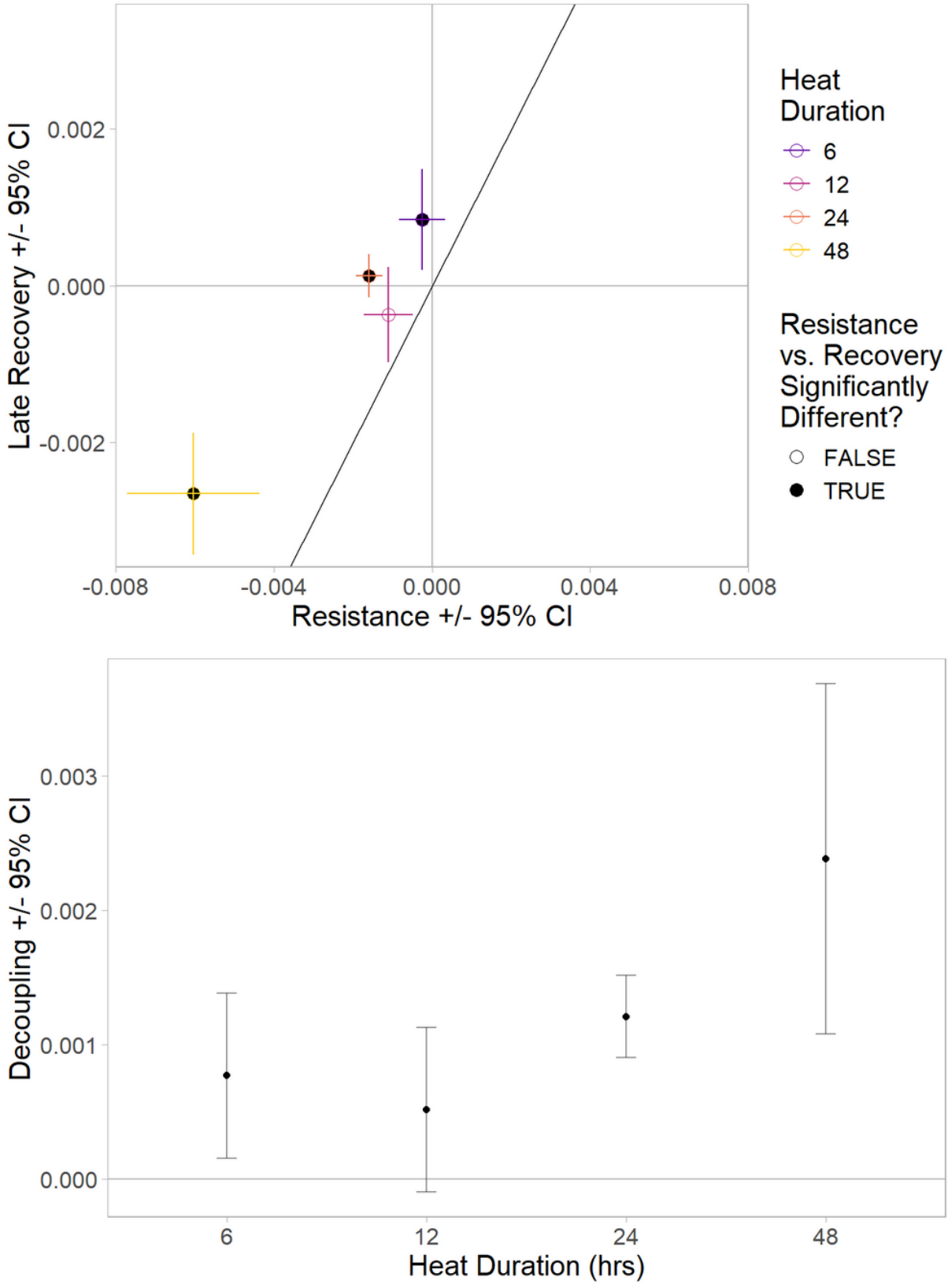

Figure S14. Decoupling plot of the effect sizes on productivity for the completely data (i.e., including communities that went extinct). The figure style is the same as Figure 5 from the main text.